NUREG/CR-4274
LA-10443-MS

Los Alamos National Laboratory is operated by the University of California for the United States Department of Energy under contract W-7405-ENG-36

Analysis and Tests on Small-Scale Shear Walls FY-82 Final Report

Los Alamos Los Alamos National Laboratory
Los Alamos, New Mexico 87545

NUREG/CR-4274
LA-10443-MS

RD

Analysis and Tests on Small-Scale Shear Walls FY-82 Final Report

E. G. Endebrock
R. C. Dove*
W. E. Dunwoody

Manuscript submitted: May 1985
Date published: September 1985

Prepared for
Mechanical/Structural Engineering Branch
Division of Engineering Technology
Office of Nuclear Regulatory Research
US Nuclear Regulatory Commission
Washington, DC 20555

NRC FIN No. A7221

*Consultant at Los Alamos. Box 725, Sandia Park, NM 87047.

Los Alamos National Laboratory
Los Alamos, New Mexico 87545

CONTENTS

TABLES

FIGURES

ANALYSIS AND TESTS ON SMALL-SCALE SHEAR WALLS
FY-82 FINAL REPORT

by

E. G. Endebrock, R. C. Dove, W. E. Dunwoody

ABSTRACT

The Phase-I experimental program was completed during FY 1982. This report summarizes the results of (1) quasi-static (monotonic and load-cycling) tests, (2) sinusoidal vibration tests, and (3) simulated earthquake tests conducted on small-scale, reinforced-concrete shear walls. Model construction, test methods, instrumentation, and experimental results are presented in this report. Experimental results are interpreted to investigate the effects of high-load levels (which produce cracking and failure of the walls) on stiffness, damping, and on deformation and acceleration transmissibility. The nonlinear analysis method that has been developed as part of this program has been used to aid in the interpretation of these experimental results.

I. INTRODUCTION

The purpose of the Structural Margins-to-Failure Program is to obtain information needed to make more reliable assessments of the margins to failure of seismic Category-I nuclear power plant structures.

The program described in this report is sponsored by the Mechanical/Structural Engineering Branch, Division of Engineering Technology of the Nuclear Regulatory Commission (NRC). This project is part of a larger NRC program designed to increase confidence in the assessment of Category-I nuclear power plant structural behavior beyond the design limit.

The structures of interest are those that are essential to the function of the safety class systems and components, or that house, support, or protect

safety class systems and components, and whose failure could lead to loss of function of the safety class system and components housed, supported, or protected.

Seismic Category-I structures are designed for specific loadings and load combinations and, because of the magnitudes of the load factors used in the design procedures, these Category-I structures would not go beyond the effective elastic limit if subjected to these original design loads. However, as plant operating experience increases, load definitions are changed or additional loadings may be prescribed; if the redefined loads were applied to the structure, the behavior may then be nonlinear. The amount of reserve strength between the structure's original design limit and the load at which the structure can no longer perform its function then becomes an important consideration. Because structural behavior beyond the original design is nonlinear, traditional structural analysis methods do not apply. The goal of this program is to obtain information on the behavior of Category-I structures at loads higher than the original design limit, primarily through experimental testing.

A detailed program plan for an investigation of the "Margins to Failure of Category-I Reinforced-Concrete Structures" is presented in Ref. 1. This program plan points out that one of the structural elements most frequently used in Category-I nuclear structures is the reinforced-concrete shear wall. The program plan then proceeds to outline a three-phase program involving tests and analysis. The Phase-I experiments, which are discussed in this report, were conducted on small, one- and two-story, reinforced, microconcrete shear wall structures that could be statically and dynamically tested to failure.

In this discussion of the Phase-I structures (small, reinforced, microconcrete shear walls), it is important to emphasize the purpose of these Phase-I experiments. These structures are <u>not</u> intended to serve as scale models of any larger structures. Hence, we do not intend to predict failure loads, crack patterns, etc., for any particular prototype structures from the results obtained from these tests. Rather, these Phase-I structures were designed to exhibit prototypical behavior on a macroscopic scale; that is, they were designed to exhibit under cyclic loading, the nonlinear, softening, hysteretic, stiffness-degradation characteristics that have been observed in prototypical shear walls.[2,3] The purpose of these tests was to develop an understanding of this nonlinear behavior and to aid in planning additional experiments.

II. DESCRIPTION OF STRUCTURES, TEST FACILITIES, AND TEST PROCEDURES

The Phase-I experiments were conducted using the small one- and two-story shear-wall structures shown in Fig. 1. The microconcrete used can be characterized as follows:

- compressive strength (f'_c), 4000-7500 psi;
- tensile strength (f_t), = 9-15% of f'_c; and
- modulus (E), 3-4 $\times 10^6$ psi.

See Fig. 2 for a typical stress vs strain diagram of sample microconcrete cylinders and Table I for a tabulation of properties and details of the mix.

As shown in Fig. 3, the reinforcement ratio of the wall section of each test structure was 0.28% (each direction and each face). The wire mesh used was a nonwoven, galvanized hardware cloth having a wire diameter of 0.042 in. and a 0.50-in. square mesh. The ultimate tensile strength was determined to be about 67 000 psi and the modulus of elasticity was about 27 x 10^6 psi.

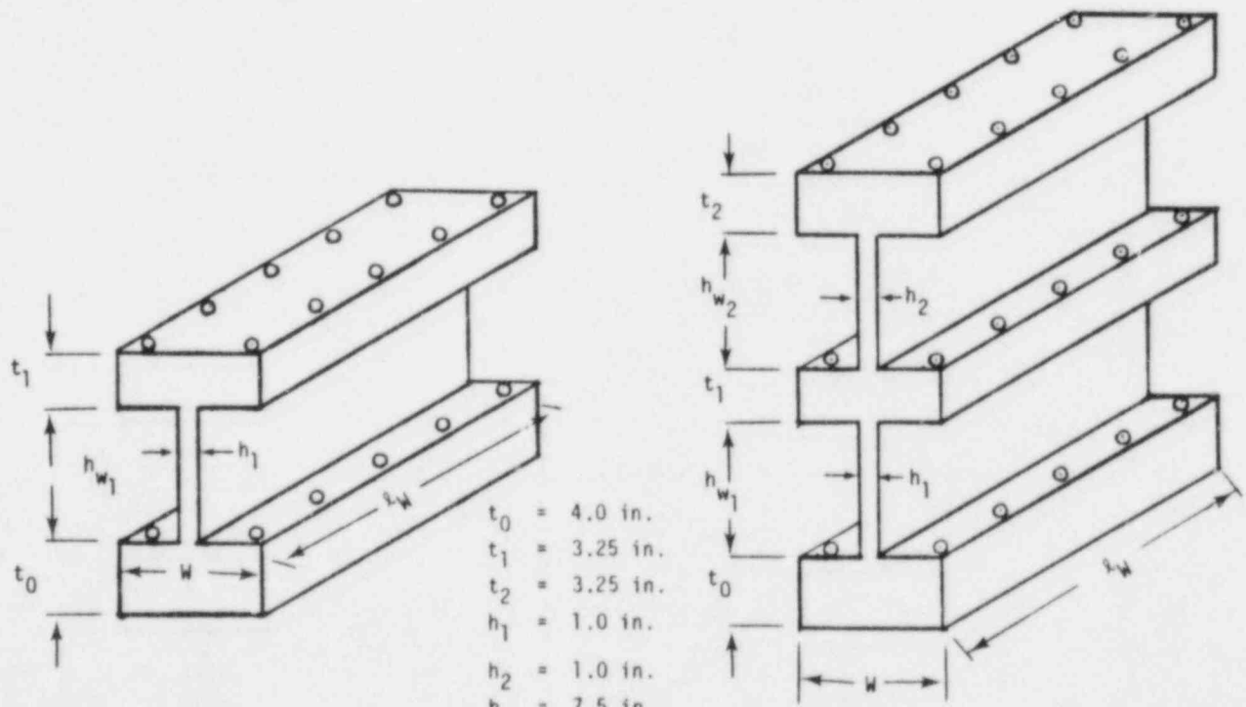

(a) One-story shear wall

(b) Two-story shear wall

t_0 = 4.0 in.
t_1 = 3.25 in.
t_2 = 3.25 in.
h_1 = 1.0 in.
h_2 = 1.0 in.
h_{w_1} = 7.5 in.
h_{w_2} = 7.5 in.
ℓ_w = 18.0 in.
w = 8.0 in.

Fig. 1. Model structures.

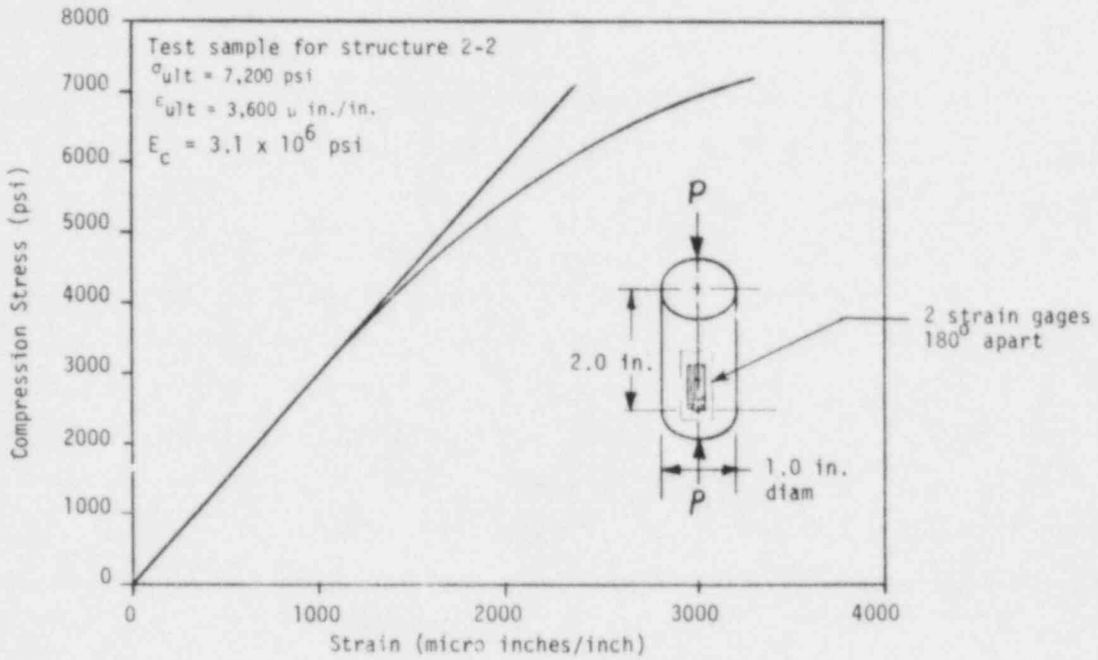

Fig. 2. Typical stress-strain diagram for microconcrete test cylinders.

Stress vs strain data for the wire are shown in Fig. 4 and pertinent data are given in Table II. Pullout tests, to investigate microconcrete/reinforcement bond strength, or "bonded tensile specimen" tests, to investigate cracking similarity (between wire-reinforced microconcrete models and standard bar-reinforced concrete prototypes), were not conducted. These subjects have been carefully studied by others[4] and the techniques required to obtain good similarity between a small model and a given prototype are well known.

Property data were not taken on the No. 3 rebar used to reinforce the top and bottom flanges of the test structures (Fig. 3) because these sections were deliberately designed to be extra strong so that they would not affect the test results. Property data for the threaded rods placed at the two ends of the wall for moment reinforcement are given in Table II. Three single-story models were constructed using twice the amount of moment reinforcement shown in Fig. 3 (that is, two 10-32 rods at each end of the models); these three models were tested quasistatically and the effect of the greater moment reinforcing is discussed in Sec. III of this report.

TABLE I

MICROCONCRETE PROPERTIES FROM COMPRESSION TESTS ON 1.00-INCH-DIAMETER BY 2.00-INCH-LONG TEST CYLINDERS

Structure No.	f'_c (Ksi)	f_t (Ksi)	E (psi)	Mix No.
1	4.34	0.65	3.0×10^6	A
2	5.89	0.64		A
3	7.35	0.69	3.6×10^6	A
4	6.86	0.67		A
5	6.31	0.68	3.4×10^6	A
10	7.48	0.85	3.5×10^6	A
11	6.27	0.66	3.4×10^6	A
12	5.74	0.72	3.0×10^6	A
13	6.85	0.72	3.4×10^6	A
21	7.18	0.97	3.9×10^6	A-1
23	5.32	0.62	3.1×10^6	B
2-2	7.45	0.89	3.1×10^6	A-1

Notes:

f'_c--computed as $f'_c(\text{Ksi}) = P/\pi d^2/4$, in which P is the maximum load developed in an axial compression test and d is the test cylinder diameter.

f_t--computed as $f_t(\text{Ksi}) = 2P/\pi \ell d$, in which P is the maximum load developed in a split cylinder test, ℓ is the cylinder length, and d is the cylinder diameter; f'_c and f_t values are averages of 5 tests.

E--modulus of elasticity; tangent modulus taken from a stress-strain diagram for a test cylinder. See Fig. 2 for example.

CONCRETE MIX

Mix No.	w/c	Water (Pounds)	Cement (Pounds)	Sand (Pounds)	Remarks
A	0.73	19	26 Type III	70	High early strength cement
A-1	0.73	19	26 Type I	70	Standard cement
B	1.00	19	19 Type I	70	Low strength mix

Notes:

1. Through holes in top and bottom flanges not shown.
2. Group II (specimens No. 4 and No. 5) as shown in figure.
3. Group I (specimen Nos. 1, 2, and 3) differ as follows: two, 10-32 steel rods at each end of web and double layer of mesh at the web/flange joints.

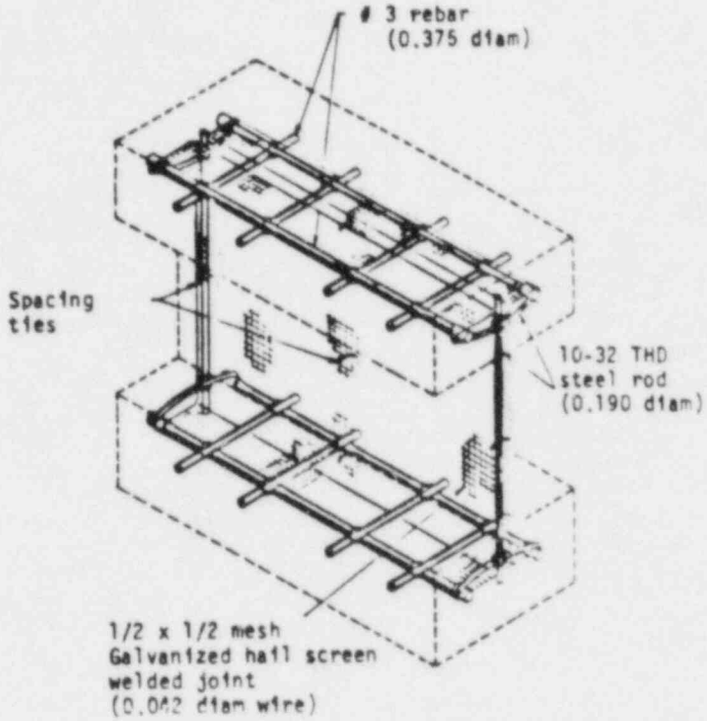

Fig. 3. Reinforcement details.

TABLE II
REINFORCEMENT MATERIAL PROPERTIES

Material (psi)	σ_{ult} (psi)	e_{ult} (%)	E (psi)
Wire mesh Lot 1	67 000	3.4	22.3×10^6
Wire mesh Lot 2	66 500	7.7	26.9×10^6
10-32 threaded steel rod used for moment reinforcement	90 500	4.2	26.3×10^6

Note: E-modulus of elasticity determined in a tensile test using a 2.000-in. gauge-length extensometer.

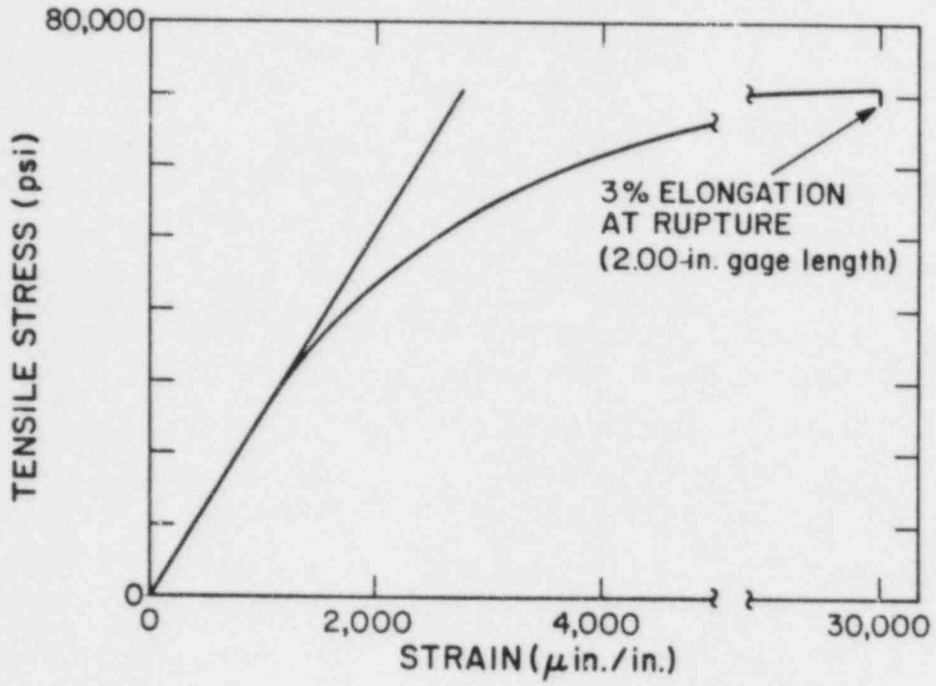

Fig. 4a. Stress-strain diagram.
Lot No. 1 wire mesh.

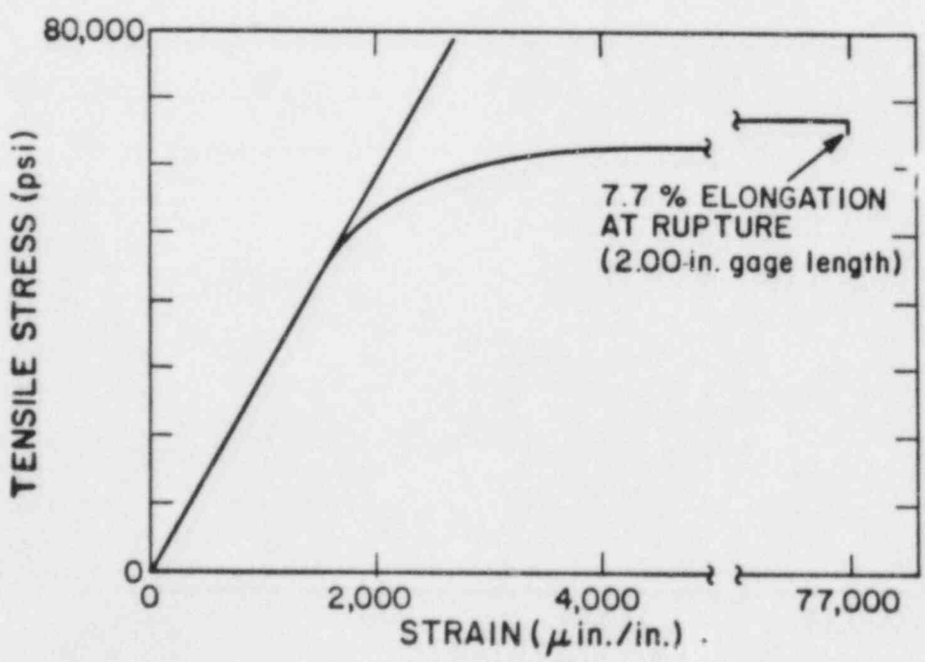

Fig. 4b. Stress-strain diagram.
Lot No. 2 wire mesh.

The single-story Phase-I specimens were quasistatically tested in a frame that is shown, schematically, in Fig. 5. In these tests, the load (monotonic or cyclic) is applied to the top flange of the shear wall by a double-acting, 20 000 lb hydraulic cylinder. The cylinder may be operated in either force control or displacement control mode and the load vs time record may be controlled manually or preprogrammed on a control tape. A rigid frame is clamped to the upper surface of the lower flange as shown in Fig. 5. This frame supports the six, marked (1-6), direct-current, variable-transformer (DCVT) displacement transducers that measure the horizontal movement of the shear wall relative to the base of the wall. The data recorded are plotted as load vs relative deformation diagrams.

For the sine-sweep and simulated seismic tests, the Phase-I structures were mounted on a horizontal slip table that is driven by a 20 000 lb force electrodynamic shaker. Figure 6 is a photograph of a one-story structure mounted and ready for test. The table, and hence the structure base, is subjected to a controlled accelerogram in the horizontal (parallel to the wall) direction. Both transverse bending and rotation about a vertical axis are excited by cross coupling of modes and the resultant transverse motion must be eliminated if the wall is to be subjected to pure shear and bending resulting

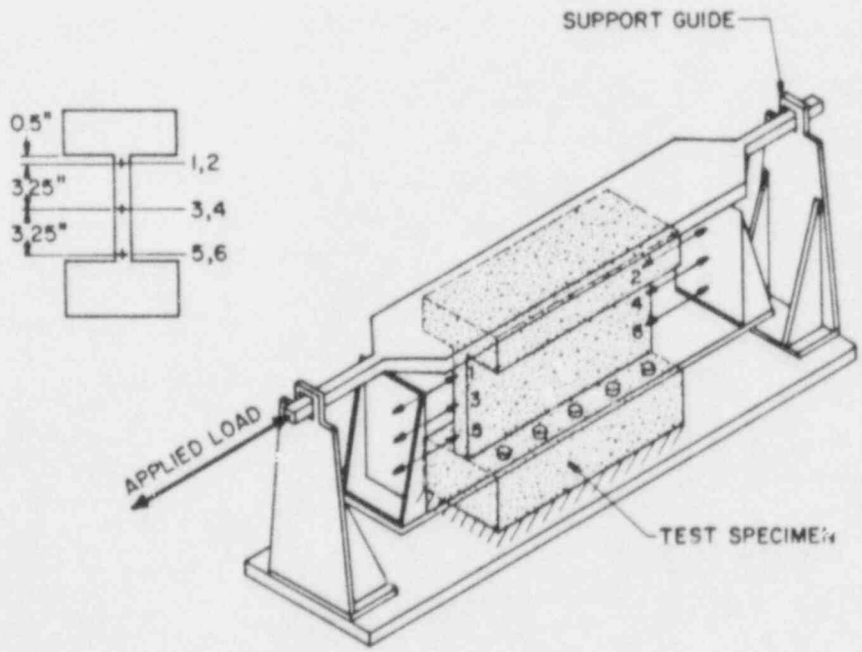

Fig. 5. Loading frame, Phase-I tests.

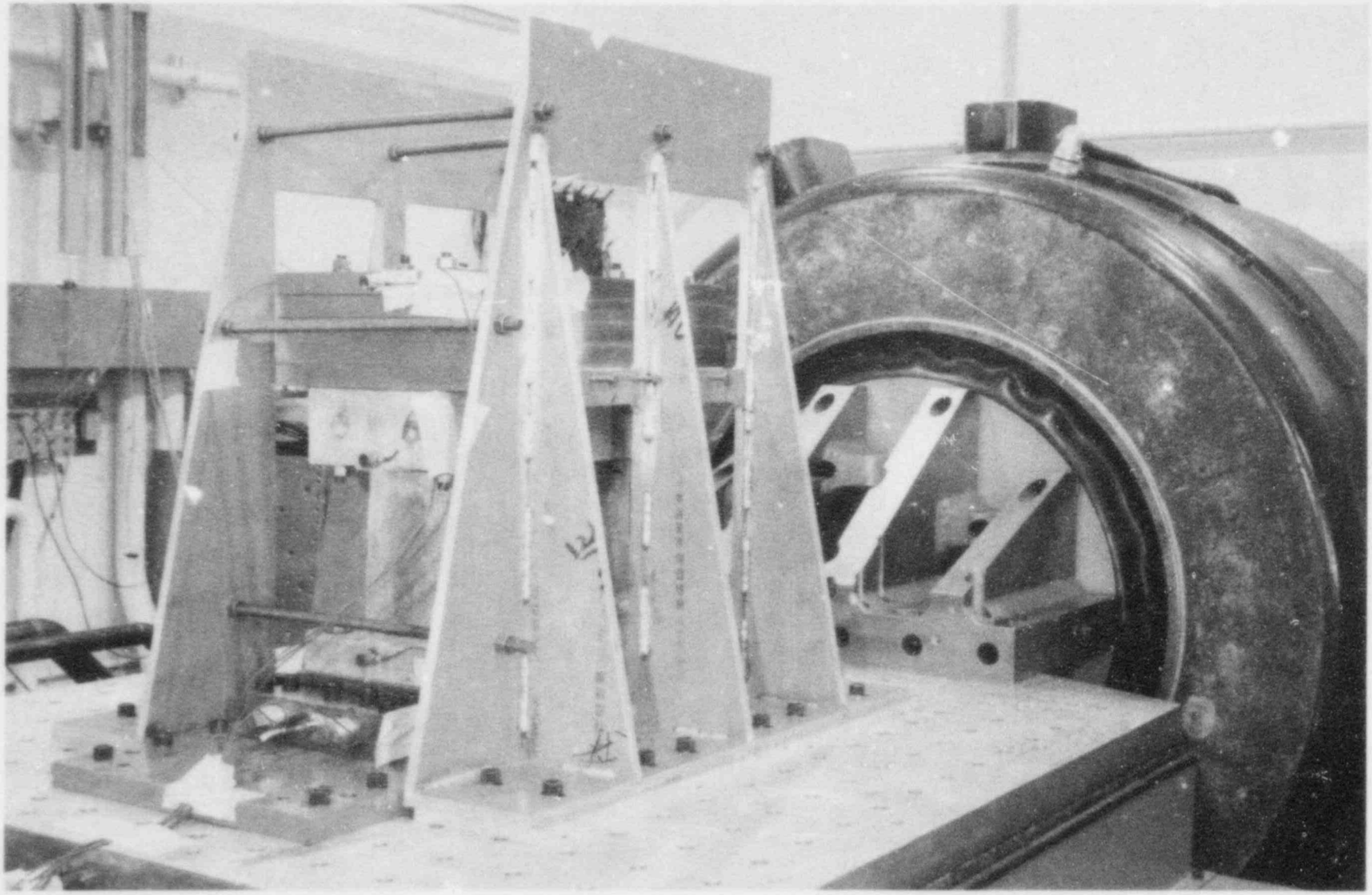

Fig. 6. Vibration test set-up for a single-story test structure.

from horizontal motions. The transverse motion is eliminated by positioning bushings that are carried by a restraining frame that surrounds the structure, so that only horizontal motion can occur. Figure 7 shows the restraining frame and a two-story structure in more detail. The mass carried by the wall consists of steel plates attached to the middle and top flanges.

During preliminary vibration testing, accelerometers were used to monitor the structure's response at various locations (top and bottom of wall, both ends of wall, top of added mass, bottom of added mass) and in three orthogonal directions (horizontal, transverse and vertical). All accelerometers were monitored to insure that horizontal motion was the controlling factor in the structural response. The primary data recorded during the actual tests were horizontal base acceleration vs time ($\ddot{Y}$, input), and horizontal acceleration of the masses attached to the middle and top flanges vs time ($\ddot{X}_1$ and $\ddot{X}_2$, response). These data are available as accelerograms and from these, absolute

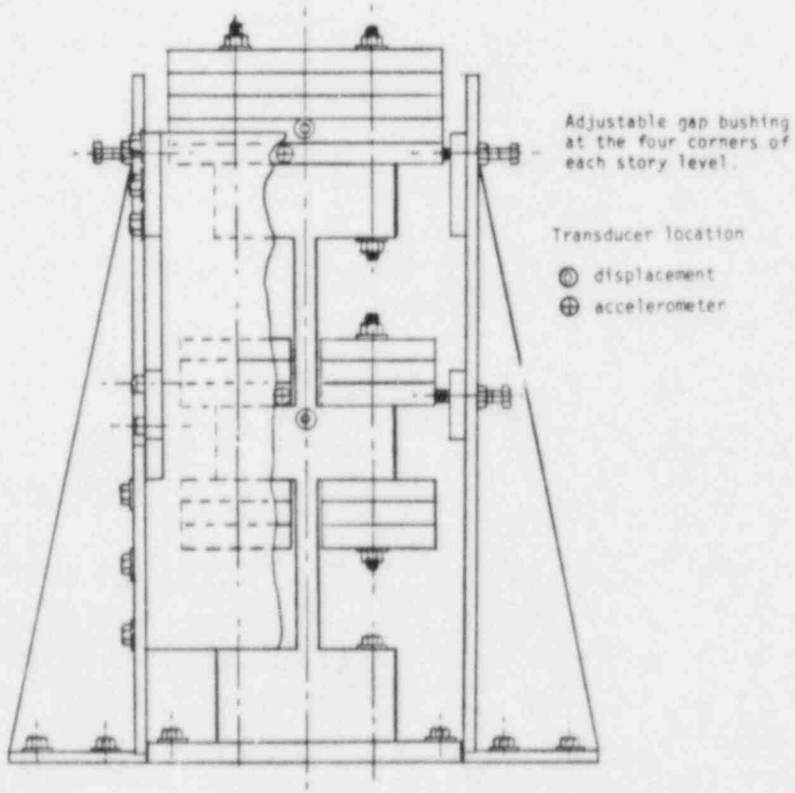

Fig. 7. Detail of restraining frame and two-story structure.

transmissibility diagrams ($\ddot{X}/\ddot{Y}$) have been plotted using a dual-channel spectrum analyzer. Additionally, the displacements of the middle and top flanges relative to the base (U_1 and U_2) were measured during the simulated seismic tests.

In the first series of tests, four single-story structures were tested to failure by subjecting each to a series of sinusoidal motion frequency sweeps (a "sine-sweep"). During each sine-sweep test, the response acceleration ($\ddot{X}$) was held at a fixed level; this level was raised with each successive sine-sweep test until failure occurred.

In the second series of tests, the structures were subjected to simulated seismic excitation; each structure was subjected to an appropriately scaled earthquake accelerogram. For this series, test procedure was as follows. For a given model structure an accelerogram, which is a frequency-scaled version of the chosen earthquake accelerogram, is selected. Starting with a small peak acceleration ($\ddot{Y}_{PK}$), tests are repeated with progresssively increasing values of $\ddot{Y}_{PK}$. The selected earthquake accelerogram and the frequency scaling involved are discussed in detail in Section V, "Simulated Seismic Tests."

III. QUASISTATIC TESTS

The five Phase-I test structures can be divided into two groups. Test structures Nos. 1-3 were fabricated using two threaded rods at each end of the wall and a double layer of wire mesh at the junctions of the wall with the top and bottom flanges (note No. 3 on Fig. 3). These specimens, which will be called Group I, have a large amount of moment reinforcement and a strengthened joint at the upper and lower ends of the wall. Group-II specimens, Nos. 4 and 5, are fabricated just as shown in Fig. 3 and, consequently, have less moment reinforcement and relatively weaker joints.

The Group-I specimens were tested in the order below:

Specimen No. 1	cyclic load test, load level increased by a 500-lb increment at the end of each full cycle,
Specimen No. 2	monotonic load test, and
Specimen No. 3	cyclic-load test, multiple cycles at each load level, Fig. 8.

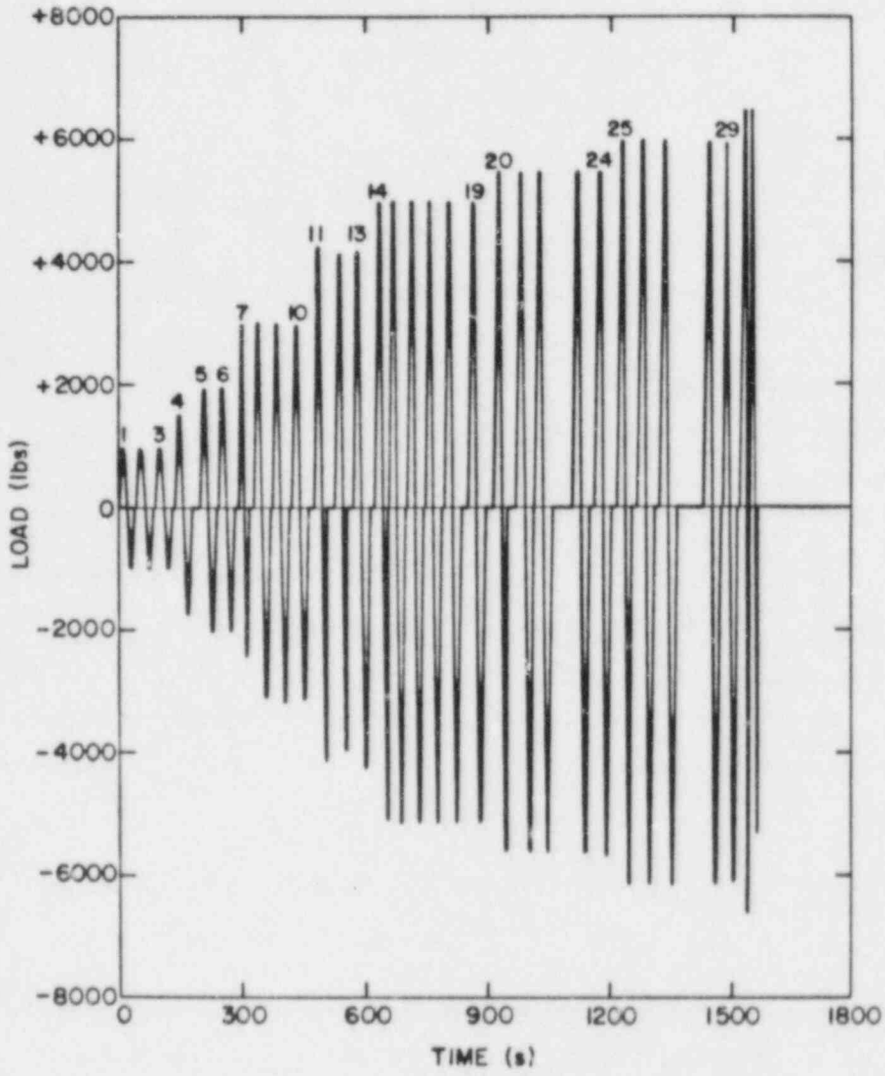

Fig. 8. Loading history, specimen No. 3.

Displacement data were recorded at six locations (points 1-6 on Fig. 5) and were plotted vs load. These raw data were then replotted as d_1-d_5, d_3-d_5, d_2-d_6, and d_4-d_6 vs load. The subtraction of d_5 from the other two displacement readings at the left end of the wall and of d_6 from the other two displacement readings at the right end of the wall eliminates lateral displacement caused by motion of the wall relative to the lower flange. Thus, $d_1' = d_1 - d_5$, $d_3' = d_3 - d_5$, $d_2' = d_2 - d_6$, and $d'_4 = d_4 - d_6$ represent wall distortion only. The displacements at the opposite ends of the wall (d_1' and d_3' or d_2' and d_4') are not identical. The end of the wall that is in a state of tension (vertically) because of the applied moment shows a larger

horizontal displacement than the end of the wall that is in a state of compression; this difference is shown in Fig. 9. During cyclic loading, the end undergoing the larger displacement reverses during each cycle except that at loads approaching the utlimate load, this pattern may be altered by the effect of opening cracks. If the wall deformation were a linear function of distance from the lower flange, we would expect d_1' to be related to d_3' (and also, d_2' related to d_4') in a linear manner. As shown in Fig. 10, this is approximately true; however, at large loads, cracking alters this linearity.

Data from all three of the Group-I tests can be summarized by plotting d_1' vs load from all three tests on the same diagram (Fig. 11). All the data from the monotonic load test are reproduced. During the two cyclic-load tests the data were continuously recorded; however, for clarity, only the enveloping curves for the increasing portion of each load cycle are shown in Fig. 11.

We can draw the following conclusions from Fig. 11.

(1) The force-deflection diagrams for all three walls have a nearly linear region below a load level of 3500 lbs. When the displacement scale is expanded it is apparent that there is no truly linear region; therefore, the 3500-lb load represents only an arbitrary point below which the nonlinearity is small compared with that exhibited at larger loads.

(2) In the linear region, specimen No. 3 has a slightly greater stiffness than specimen Nos. 1 and 2. Specimen No. 3 is fabricated of higher-strength concrete as indicated in Table I.

(3) The monotonically loaded wall has the highest ultimate strength, but the cyclically loaded walls experience larger deformations.

(4) When the load is smaller than the linear limit, load cycling does not produce appreciable stiffness degradation; that is, the force-deformation loop is repeatable. For larger loads, repeated cycles of load result in progressively increasing deformation at the same load; this produces the steps in the load envelope curve for specimen No. 3.

Additional insight into response to cyclic loading may be gained by studying the load-deflection time records taken from the test of specimen No. 3 that was loaded as shown in Fig. 8. These complete force-deformation (d_1')

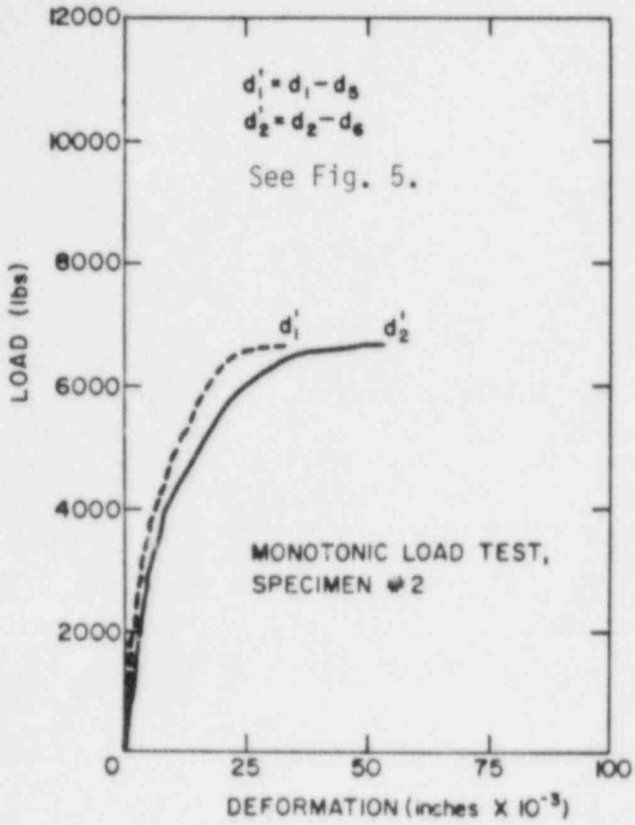

Fig. 9. Right-and left-end deformations.

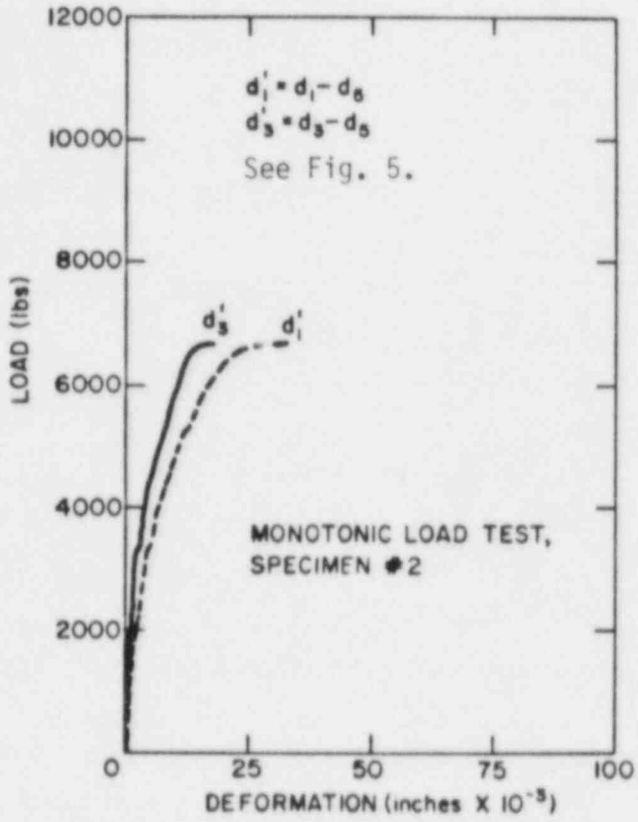

Fig. 10. Upper and midheight deformations.

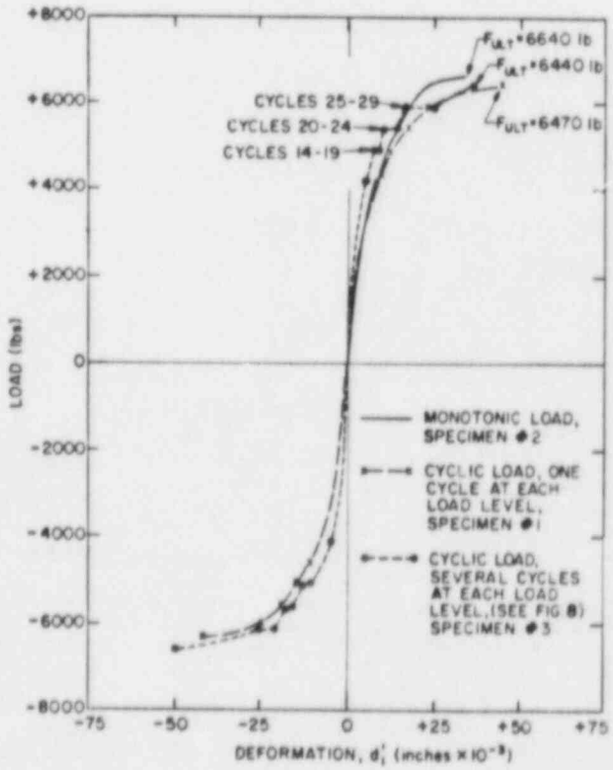

Fig. 11. Group I, test summary.

curves are shown in Fig. 12. From these figures we can make the following observations.

(1) Below the linear limit the area within the hysteresis loop is small and load cycling causes little or no stiffness degradation. Figure 12 shows the data from load cycles 7-10 overlaid to plot a single hysteretic loop.

(2) As the load level increased, the area within the hysteresis loop increased and as the load was cycled, at that load level, the deformation increased (Figs. 12b-12e). Integration of these hysteresis loops yields the energy loss per cycle at each load level. Values obtained from these integrations will be discussed in more detail later in this section.

Specimen Nos. 4 and 5 were fabricated as shown in Fig. 3, that is, a single-threaded rod at each end of the wall for moment reinforcement and a single layer of wire mesh on each side of the wall that extends into the top and bottom flanges. Hence, these two specimens, which will be referred to as Group II, had relatively less moment reinforcement and weaker wall-to-top and bottom flange joints. Group II specimens were tested as follows:

Specimen No. 4 monotonic load test, and

Specimen No. 5 cyclic-load test, repeated cycles at each load level, see Fig. 13.

The results of these two tests are summarized in Fig. 14, where the complete force-deformation curve is plotted for the monotonic load test and the envelope of the load-deformation data is plotted for the cyclic load tests. As was the case with the Group I tests, the wall loaded monotonically had the highest ultimate strength. However, unlike the Group I tests, the cyclically loaded Group II wall did not have significantly greater maximum deformation at failure than the monotonically loaded wall.

As was the case with the Group I specimens, both of the Group II specimens had a linear region in their force-deformation diagrams with the linear limit at approximately 3500 lbs. Below this limit load, cycling did not produce significant stiffness degradation.

Comparison of the data presented in Fig. 11 (Group I, large moment reinforcement) with those presented in Fig. 14 (Group-II, small-moment reinforcement) reveals the differences in these two groups of specimens. The two monotonically loaded walls had nearly identical ultimate strengths; however, the

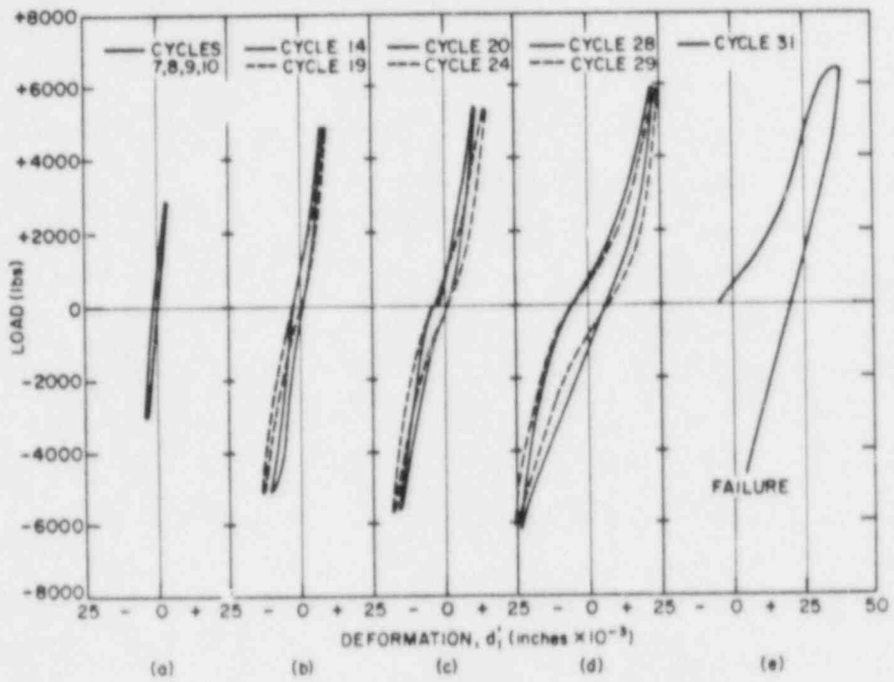

Fig. 12. Cyclic-load test, specimen No. 3.

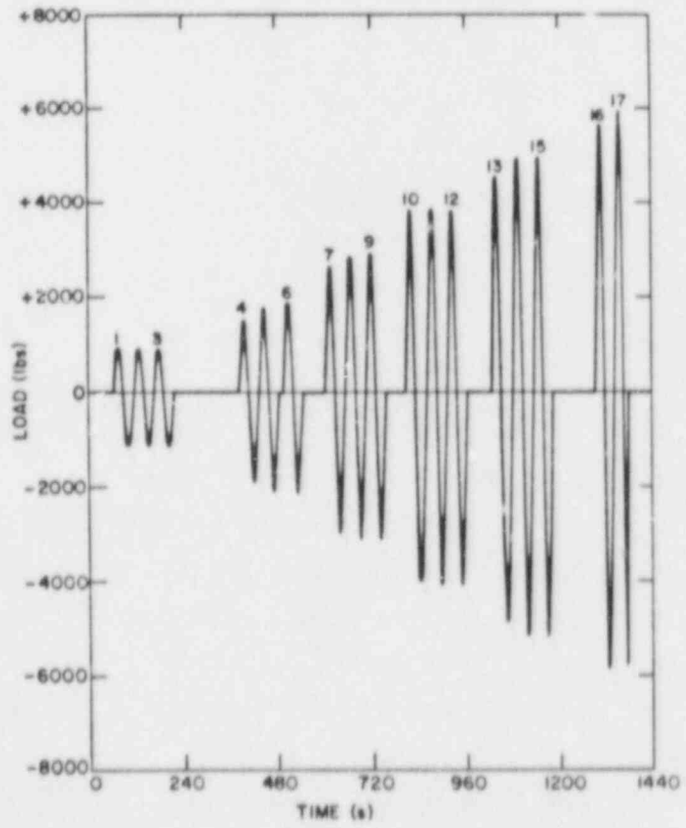

Fig. 13. Loading history, specimen No. 5.

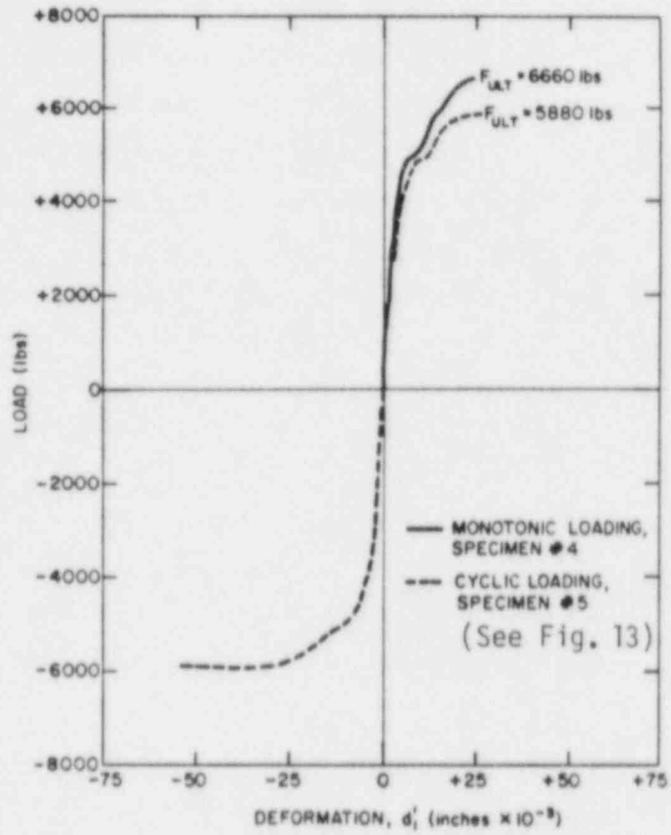

Fig. 14. Group II, test summary.

maximum deformation was greatly reduced in the Group II wall. Under cyclic loading, the Group II wall shows lower ultimate strength and maximum deformation than the Group I walls.

In addition to the differences between the two groups of specimens discussed in the preceding paragraph, other differences are obvious from a visual examination of the failed specimens. In the Group I walls (large moment reinforcement), the failed walls show extensive shear cracks throughout the wall. In the Group II walls (smaller moment reinforcement), visible cracks originate as tensile cracks at either end of the wall and gradually change angle (towards 45° to the horizontal) as they propagate away from the ends of the wall. The Group II walls fail by separation of the wall from its foundation, and at failure the number of shear cracks (cracks at approximately 45° to the horizontal) is fewer than the number observed in the Group I walls.

As previously mentioned, the data from the cyclic-load tests can be integrated to find the area inside the hysteresis loops; this area is proportional to the energy loss per cycle. The results of these integrations are presented in Table III. It appears that the specimen with the smaller amount of moment reinforcement has the greater amount of energy dissipation per cyle at the higher load levels. It is impossible to rigorously relate this hysteretic energy loss to the more commonly used damping ratio, ζ, which is defined as the ratio of the viscous damping coefficient, C, to the critical value of C, defined as $C_c = 2\sqrt{KM}$. That is,

$$\zeta = \frac{C}{C_c} = \frac{C}{2\sqrt{KM}} \quad ,$$

where K and M are the system stiffness and mass respectively. One reason for this is that the system stiffness is not defined for a nonlinear system. However, it may be informative to make the following approximate calculations to relate the measured hysteretic energy losses (ΔE) to ζ.

If we assume that the response motion of a linear, viscously damped system is harmonic, the relationship between damping ratio, ζ, and energy loss per cycle, ΔE, is[5]

$$\zeta = \frac{\Delta E}{2\pi \frac{\omega}{\omega_n} \frac{F^2}{K}} \quad ,$$

in which ω/ω_n is the ratio of vibration frequency to the system's natural frequency, F is the force at the maximum deformation, and K is the system's stiffness. If we further assume that we wish to evaluate the effective damping ratio, ζ_e, at the system's natural frequency, that is, $\omega/\omega_n = 1$, we may write

$$\zeta_e = \frac{\Delta E}{2\pi \frac{F^2}{K}} \quad ,$$

TABLE III

HYSTERETIC ENERGY LOSS

A. SPECIMEN NO. 3 - GROUP I, LARGE-MOMENT REINFORCEMENT

Cycle No. (Fig. 8)	ΔE (in.-lb/cycle)	F_{pk} (lb)	K_s (1) (lb/in.x10^6)	ζ_e (2) (%)
7	3	3000	1.09	5.8
11	10	4240	0.77	6.8
14	21	4920	0.65	9.0
19	23	4920	0.62	9.4
26	62	5920	0.31	8.7
28	68	5920	0.25	7.7

B. SPECIMEN NO. 5 - GROUP II, SMALL-MOMENT REINFORCEMENT

Cycle No. (Fig. 13)	ΔE (in.-lb/cycle)	F_{pk} (lb)	K_s (1) (lb/in.x10^6)	ζ_e (2) (%)
7	2	2740	1.18	5.0
10	7	3880	0.87	6.4
13	18	4640	0.67	8.9
15	40	4960	0.42	10.9
16	126	5600	0.34	21.7
17	173	5880	0.23	18.3

(1) K_s is the secant stiffness modulus at the corresponding peak force, that is, the slope of the straight line joining the origin and the extreme peak of the positive hysteretic loop.

(2) ζ_e is computed as $\zeta_e = \Delta E \times K/2\pi F^2$; see text for a discussion of the numerous assumptions involved.

and solve for the effective damping ratio, ζ_e, of any energy loss, ΔE. We substitute the peak force, F, of the cycle associated with that energy loss and the secant stiffness modulus (K_s) at that force level for K; the results of this calculation are given in Table III.

The reader is reminded that the assumptions made in the above calculations are both numerous and questionable. At best, the computed values of the equivalent damping factor would apply only to the system vibrating at resonance, through full cycles, at a load level of $\pm$ F used in the calculation. Indeed, a linear system with an equivalent damping ratio is not a good approximation for a nonlinear-hysteretic system acted upon by seismic excitation.

A complete summary of the date, together with ultimate and first cracking loads, and initial stiffness computed using the usual design equations are presented in Table IV.

TABLE IV
DATA SUMMARY

GROUP-I, LARGE-MOMENT REINFORCEMENT (SEE FIG. 3)

Specimen No. and Load Condition	Δ (1) (in.x10^{-3})	K_1 (2) (lb/in.x10^6)	F_{ULT} (3) (lb)	U_{ULT} (4) (in.x10^{-3})	$\mu = \frac{U_{ULT}}{\Delta}$	V_u (5) (lb)	V_{CR} (6) (lb)	$K_{calc.}$ (7) (lb/in. x 10^6)
No. 2, Monotonic	4.5	0.79	6640	32	7.2	5320	3650	2.71
No. 1, Cyclic	4.5	0.78	6470	44	9.8	4870	3770	2.33
No. 3, Cyclic	3.2	1.0	6440	38	11.9	5630	3760	3.03

GROUP-II, SMALL-MOMENT REINFORCEMENT (SEE FIG. 3)

Specimen No. and Load Condition	Δ (1) (in.x10^{-3})	K_1 (2) (lb/in.x10^6)	F_{ULT} (3) (lb)	U_{ULT} (4) (in.x10^{-3})	$\mu = \frac{U_{ULT}}{\Delta}$	V_u (5) (lb)	V_{CR} (6) (lb)	$K_{calc.}$ (7) (lb/in. x 10^6)
No. 4, Monotonic	3.3	1.06	6660	22	6.8	5570	3650	2.92
No. 5, Cyclic	4.0	0.87	5880	26	6.5	5390	3710	2.80

(1) Δ - d_1' at a load of 3500 lb.
(2) K_1 - stiffness modulus in linear region.
(3) F_{ULT} - maximum positive load, last complete cycle.
(4) U_{ULT} - d_1' at F_{ULT}.
(5) V_u - ultimate strength computed using ACI 349.
(6) V_{CR} - cracking strength computed using ACI 349.
(7) $K_{calc.}$ - calculated stiffness, includes flexural and shear deformations.

Perhaps the most important observations are the following: (1) these small specimens behave very much as do larger specimens that have been tested by others,[2,3] (2) the measured stiffness (K) was found to be considerably less than the calculated values, and (3) the measured ultimate strengths (F_{ult}) were found to be slightly larger than the calculated values (V_u).

IV. SINE-SWEEP VIBRATION TESTS

All four one-story Phase-I structures subjected to sine-sweep vibration tests were Group II (low moment reinforcement, see Fig. 3) specimens. This choice was made because this lesser amount of moment reinforcement was more typical of the walls of interest in this research.

As mentioned in Section II of this report, these sine-sweep vibration tests were conducted by selecting the desired peak response acceleration level ($\ddot{X}_{pk}$) and holding the level constant (using a servocontrol) while the frequency (ω) was swept through the apparent resonant frequency of the system. The value selected for $\ddot{X}_{pk}$ was increased after each sweep test and the frequency sweep repeated until failure occurred. Tests were conducted in this manner (that is, peak-response acceleration, $\ddot{X}_{pk}$, held constant) in an attempt to determine the apparent resonant frequency of the system at a specified constant value of peak shear force (which is proportional to peak response acceleration).*

During these tests the principal data recorded were:

1. the input horizontal acceleration ($\ddot{Y}$) as measured by an accelerometer mounted on the base plate to which the structure is attached, and
2. the response horizontal acceleration ($\ddot{X}$) as measured by an accelerometer mounted on the steel mass that was attached to the top of the test structure.

These data (along with a considerable amount of additional data from accelerometers at other locations) were recorded on tape. The principal

*With linear systems it is customary to do sine-sweep vibration tests in which the peak input, or base, acceleration, $\ddot{Y}_{pk}$, is held constant. In this case the peak response acceleration, $\ddot{X}_{pk}$, and spring distortion, Z, vary with frequency; however, for a linear system, the response ratio, $\ddot{X}_{pk}/\ddot{Y}_{pk}$, and the frequency at which the response ratio is maximized is assumed to be independent of the magnitude of $\ddot{X}_{pk}$ or Z. For the nonlinear system being considered in the present tests, we wish to know how response-acceleration level affects both response ratio and resonant frequency.

technique of data reduction was the transformation of acceleration-time data into the frequency domain, and the computation of acceleration transmissibility ($T_A = \ddot{X}/\ddot{Y}$), using a Nicolet Model 660 Dual Channel Spectrum Analyzer. Figure 15 shows a typical plot of input and response acceleration ($\ddot{Y}$ and $\ddot{X}$) in the frequency domain. The upper trace in Fig. 15 is a plot of the horizontal acceleration of the steel mass supported by the shear wall, that is, $\ddot{X}$, the response acceleration. Notice that this acceleration remains essentially constant over the frequency range of the test, a condition accomplished by servocontrolling the shaker to maintain this acceleration constant. As previously stated, the purpose of this type of test was to hold the response acceleration, and, hence, the shear force (F) in the wall, at a constant peak level while the frequency was varied. The lower trace in Fig. 15 is a plot of the base acceleration ($\ddot{Y}$) vs frequency.

The usual absolute acceleration transmissibility curve, constructed by dividing $\ddot{X}$ by $\ddot{Y}$ at each frequency, is shown as a solid line in Fig. 16. This transmissibility curve can be used for several purposes.

1. The system under test can be compared with a viscously (or structurally) damped, linear system by comparing this curve with the curve generated for the linear system. In Fig. 16, the dotted curve is the transmissibility curve computed for a viscously damped linear system

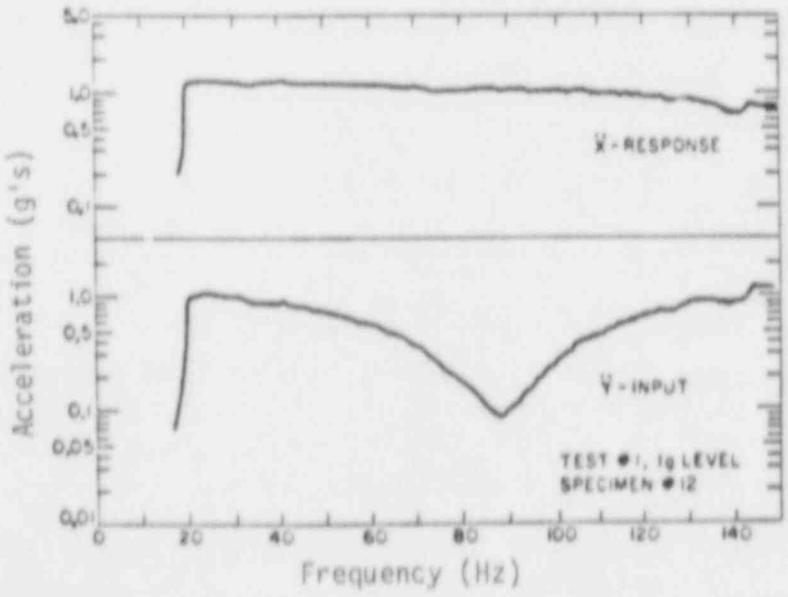

Fig. 15. Input ($\ddot{Y}$) and response ($\ddot{X}$) acceleration.

with a damping factor of 0.039. Obviously, the linear system response only approximates the actual system response.

2. Recognizing that it is only an approximation, the equivalent viscous damping ratio $\zeta_e = 1/2(\ddot{X}/\ddot{Y})max.$* Thus, for the specimen and test data shown in Fig. 16, $\zeta_e = 1/(2x12.9) = 0.039$.

3. Again, considering the system to be approximated by a linear system, the equivalent stiffness (K_e) can be computed from the measured resonant frequency (f_r) and the system mass (M). Hence, for this system and this test, and taking the mass, M, to be the mass of the steel plates plus the upper concrete flange we have

$$K_e = (2\pi f_r)^2 M$$
$$= (2\pi \times 86)^2 (300 + 40)/386$$
$$= 0.257 \times 10^6 \text{ lb/in.}$$

Because each specimen was tested at several acceleration levels, it is possible to superimpose the transmissibility diagrams plotted for each test, and, by comparison, to determine how both equivalent stiffness (K_e) and equivalent viscous damping (ζ_e) are affected by response acceleration level. This has been done for five tests on specimen No. 12, in Fig. 17, and the results are tabulated in Table V. It is obvious that for this specimen, both the equivalent stiffness (K_e) and the equivalent viscous damping ratio (ζ_e) decrease as the response acceleration ($\ddot{X}$), or load level, increases. The final test, No. 5, in which the load level was reduced to approximately the same as in test No. 2, indicates that the structural changes are irreversible.

The data from tests on four specimens (Nos. 10-13) were reduced as described in the preceding paragraphs, and the results are given in Figs. 17-20 and Table V. The data taken from the tests on specimen No. 10, which are presented in Fig. 20 and Table V, require some additional comments.

1. This specimen had a notably higher initial resonant frequency and, therefore, a larger initial equivalent stiffness.

*In linear theory, this response ratio $(\ddot{X}/\ddot{Y})_{max}$, is the steady state value. With concrete structures, a steady state is not realized, especially at high load levels, because the stiffness of the element is constantly degrading with load cycling, even if the load level is held constant. See Fig. 12.

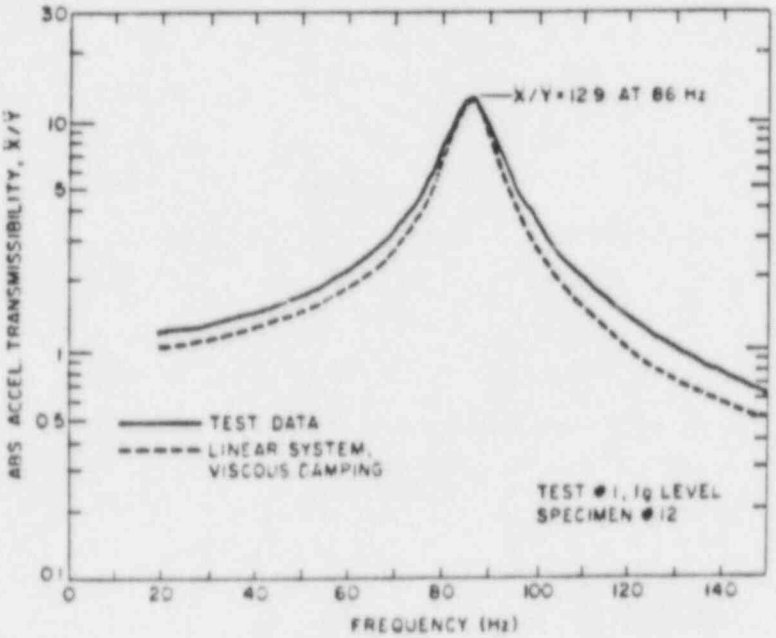

Fig. 16. Typical transmissibility diagram.

2. At a response acceleration level of 5.44 g's (test No. 3), the specimen underwent an abrupt change; note the "break" in the curve for test No. 3 on Fig. 20. At this point, visible hairline cracks appeared at the junction between the lower end of the web (the wall) and the bottom flange (the foundation).
3. After test No. 3, the specimen was tested at a response acceleration level of 5.38 g's (test No. 4) and the response was similar to that found for specimens 11-13, that is, f_r = 72 Hz.
4. Specimen No. 10 failed during test No. 5 (curve No. 5 on Fig. 20). In Fig. 21 the response acceleration ($\ddot{X}$)-time diagram is plotted for two frequencies. Figure 21a shows the shape of $\ddot{X}$ at 36 Hz, just before failure (the peak on curve No. 5 on Fig. 20). Figure 21b shows the shape of $\ddot{X}$ at 49 Hz, just after failure. The sharp acceleration spikes after failure are characteristic of impacting surfaces.

As expected, the effective stiffness (K_e), of these four walls decreases with increase in response level; however, some of the other results are somewhat surprising.

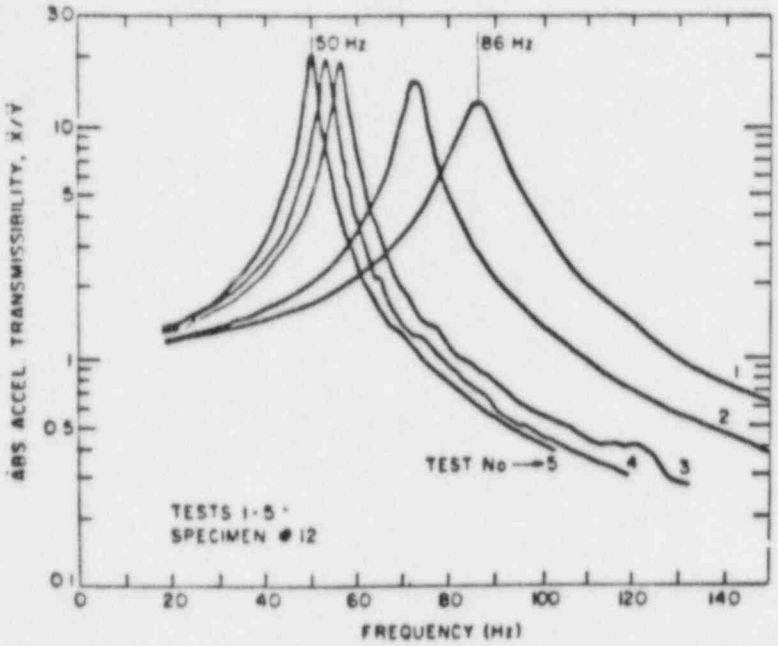

Fig. 17. Transmissibility, specimen No. 12.

1. Even at the lowest load level, the equivalent stiffness (K_e) computed from the measured resonant frequency is consistently and considerably less than the values of stiffness determined by the quasistatic tests. There may be several reasons for this difference, but the authors are currently pursuing the possibility that the low stiffness and low ultimate strength found in the vibration tests are associated with large degradation of stiffness and strength caused by load cycling. It must be remembered that, although the load level is very low during the first vibration test on each specimen, the load reversals that occur before the first resonance is reached number in the thousands. Before the specimen fails, the load reversals number in the hundreds of thousands.
2. During the quasistatic load-cycling tests, the area inside each hysteresis loop (and, consequently, the energy dissipated during each load cycle) was found to increase with both load level and number of load cycles (Fig. 12). Therefore, it was anticipated that during vibration tests, the equivalent damping would increase as the load level increased. This was indeed the case with specimens 10 and 13, as can be seen in Figs. 18 and 20 and Table V; however, specimens 11 and 12 showed that as the load level increased, the equivalent

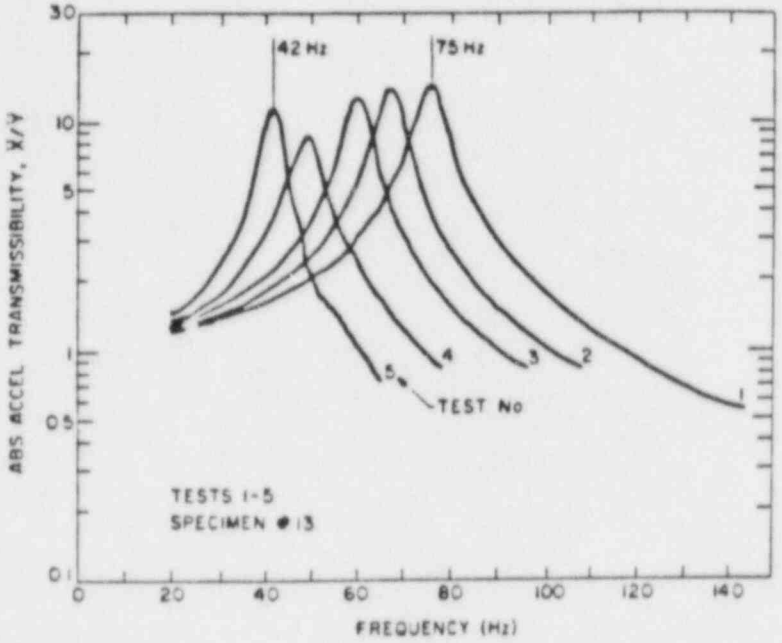

Fig. 18. Transmissibility, specimen No. 13.

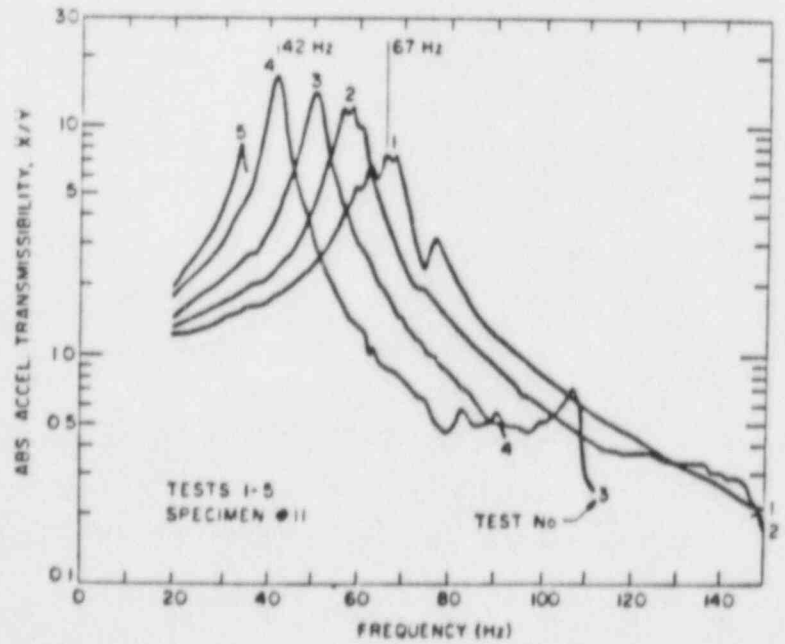

Fig. 19. Transmissibility, specimen No. 11.

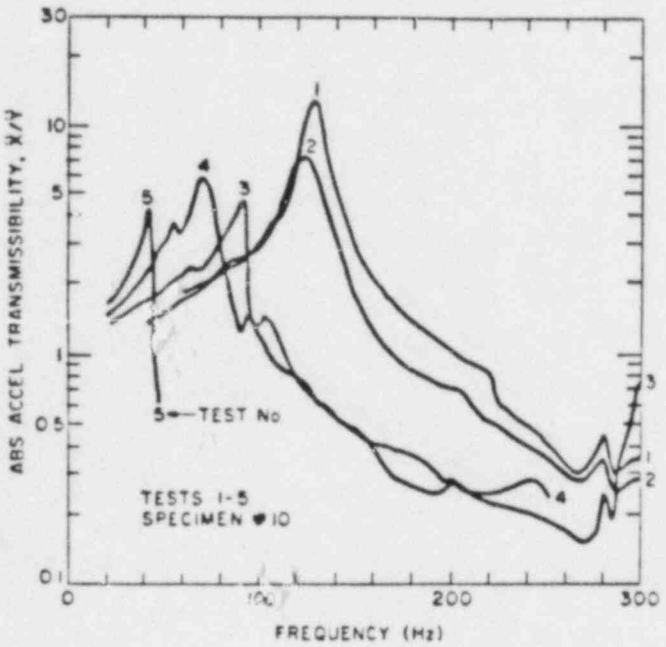

Fig. 20. Transmissibility, specimen No. 10.

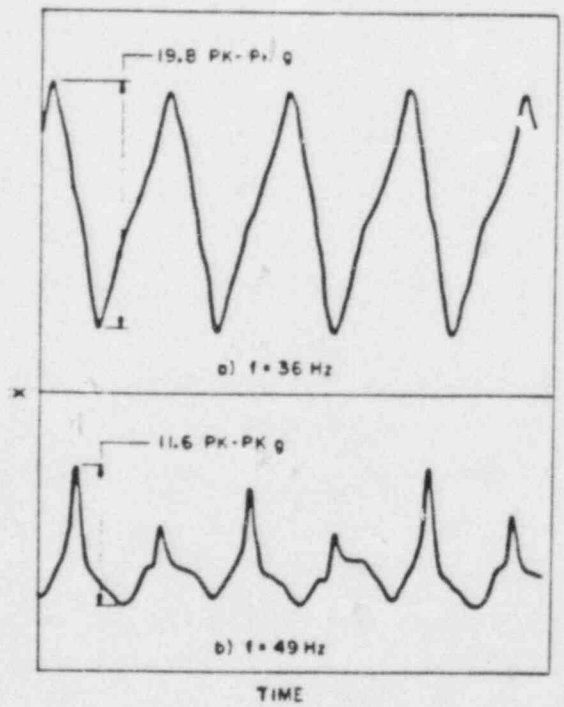

Fig. 21. Acceleration-time histories, specimen No. 10.

TABLE V

RESULTS OF SINE-SWEEP TESTS

Specimen No.	Test No.	Response Acceleration Level - $\ddot{X}$ (g's)	Shear Force - F $F = M\ddot{X} = 340\ \ddot{X}_g$ (lb)	Resonant Frequency-f_R (Hz)	Equivalent Stiffness-K_e (lb/in.x10^6)	Equivalent Viscous Damping-ζ_e (%)
12	1	1.19	404	86	0.26	3.9
	2	2.41	819	72	0.18	3.2
	3	3.55	1207	56	0.11	2.6
	4	4.59	1560	53	0.10	2.5
	5	2.33	792	50	0.09	2.4
13	1	1.21	411	75	0.20	3.4
	2	2.14	728	66	0.15	3.4
	3	3.37	1146	59	0.12	3.9
	4	4.21	1431	48	0.08	5.6
	5	5.55	1887	42	0.06	4.3
11	1	0.97	330	67	0.15	6.4
	2	1.93	655	56	0.11	4.0
	3	3.03	1029	50	0.09	3.5
	4	4.20	1426	42	0.06	2.9
	5	4.33	1471	--	--	--
10	1	0.94	320	132	0.61	3.8
	2	1.57	534	125	0.54	6.5
	3	5.44	1850	--	--	--
	4	5.38	1829	72	0.18	8.5
	5	9.90	3366	--	--	--

damping decreased (Figs. 17 and 19 and Table V). It may be that the energy dissipation mechanisms are very dependent on how concrete cracking and reinforcement failure progresses, and that these phenomena may differ from test to test, even with supposedly identical specimens.

Taking all of these sine-sweep experimental results into account, the authors now have serious doubts that it will be possible to work from the results of classical vibration tests to the prediction of earthquake response. Certainly, structural response to an earthquake involves velocity-dependent effects and, accordingly dynamic testing is required. However, structural response to an earthquake involves only a limited number of load cycles whereas many load cycles are involved in classical sinusoidal vibration testing. With concrete, difference in loading history before failure appears to be extremely important.

V. SIMULATED SEISMIC TESTS

In the final series of tests, both one- and two-story Phase I structures were subjected to simulated seismic base excitation. Figure 22 is a photograph of a two-story structure, surrounded by the torsional and transverse motion-restraining frame, mounted on the shake table ready for testing. Figure 23 is a photograph of the same structure, with the frame partially removed, after the simulated seismic test. Figure 24 shows the weight distribution and location of principal accelerometers used during these tests. Accelerations were measured at various other locations and in various directions during the course of these tests, but results are presented in terms of input and response acceleration in the in-plane direction ($\ddot{Y}$ and $\ddot{X}$). Relative displacements between the first- and second-story flanges and the surrounding frame (U_1 and U_2) were made using variable resistance and eddy-current type displacement gauges. These quantities, U_1 and U_2, represent motion of the structure relative to the base, plus or minus motion of the frame relative to the base. Measurements of frame acceleration and analysis show that at the frequencies of interest, the motion of the frame relative to the base is small compared with relative motion of the structure.

The basic accelerogram used in these tests was one that had previously been constructed so as to envelop the NRC Horizontal Design Response Spectrum. This accelerogram, called EE1, and its linear response spectrum are shown in Fig. 25. This real-time earthquake signal was then frequency (or time) scaled to produce four accelerograms with the appropriate frequency content for the small structure being tested.

Time scales (N_t) used were the following:

1. N_t = 4.96; this signal, designated as EE1 x 5, is identical in shape to the real-time signal, Fig. 25a, but with a duration of 2.42 s, that is, 12/4.96. The frequency spectra (response, Fourier, etc.) is up shifted (to the right in Fig. 25b) by a factor of 4.96.
2. N_t = 10.0; this is designated as EE1 x 10 with a duration of 1.20 s, and having a frequency content up shifted by a factor of 10.

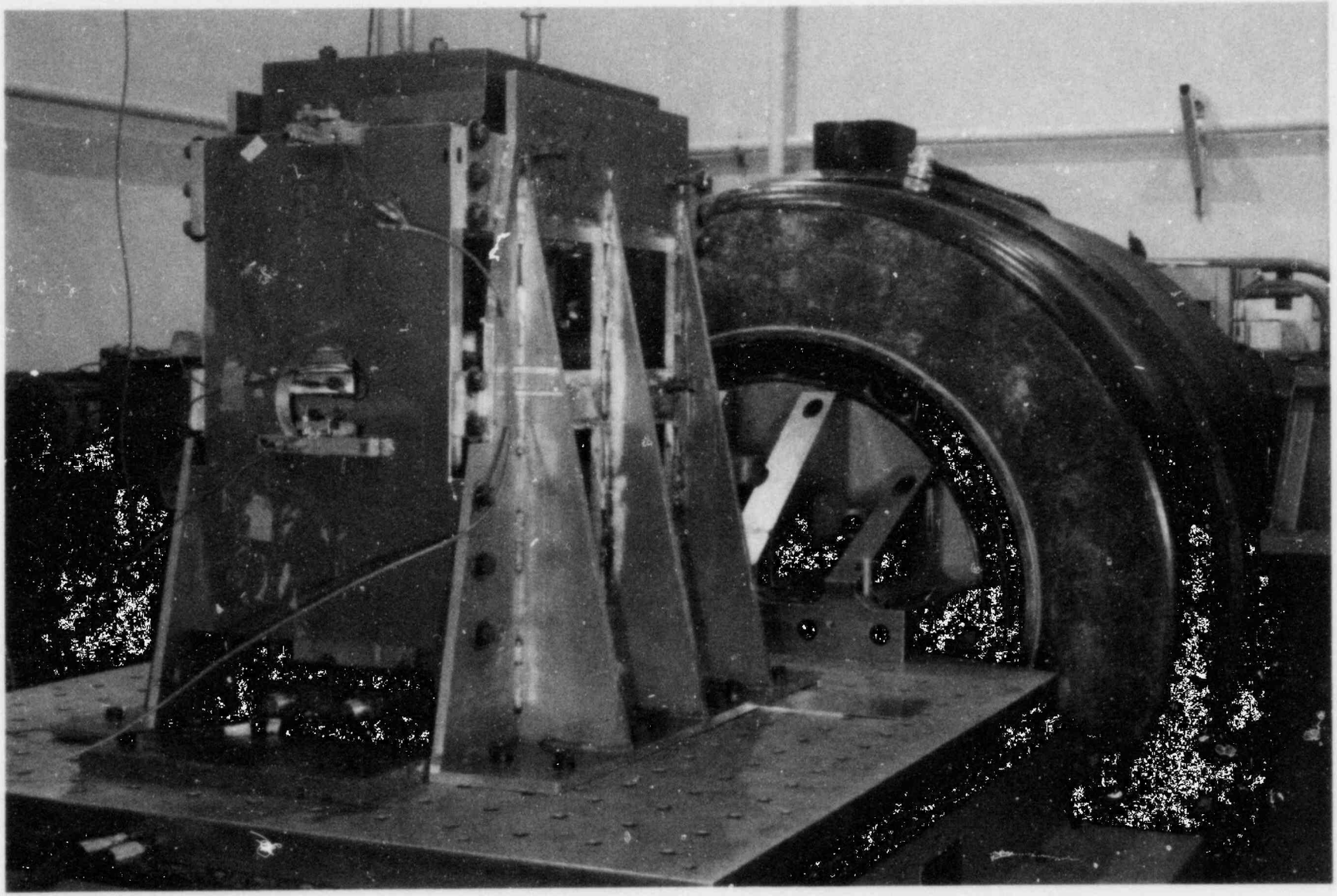

Fig. 22. Simulated seismic test set-up for a two-story shear wall structure.

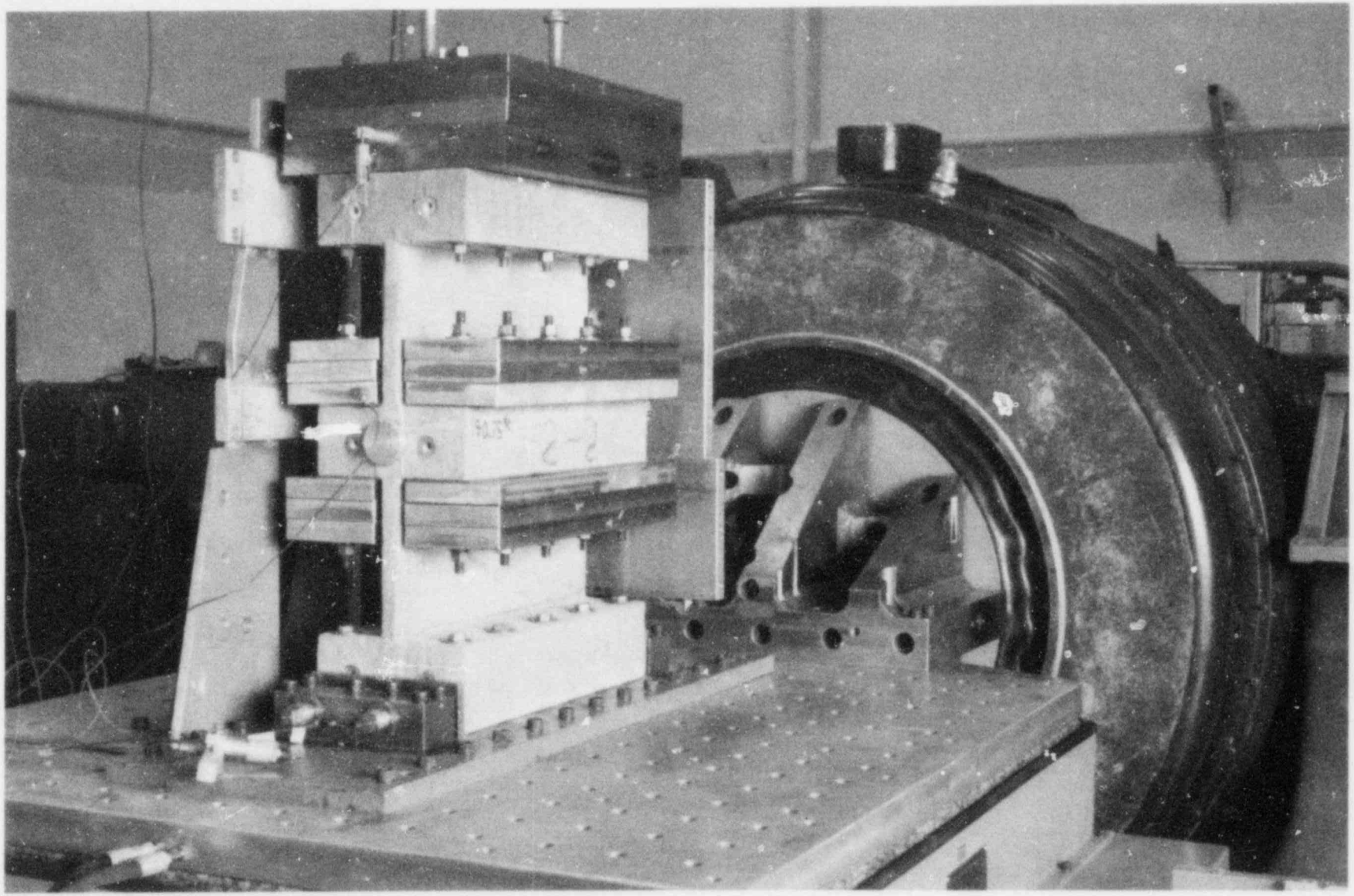

Fig. 23. Simulated seismic-damaged, two-story shear wall structure.

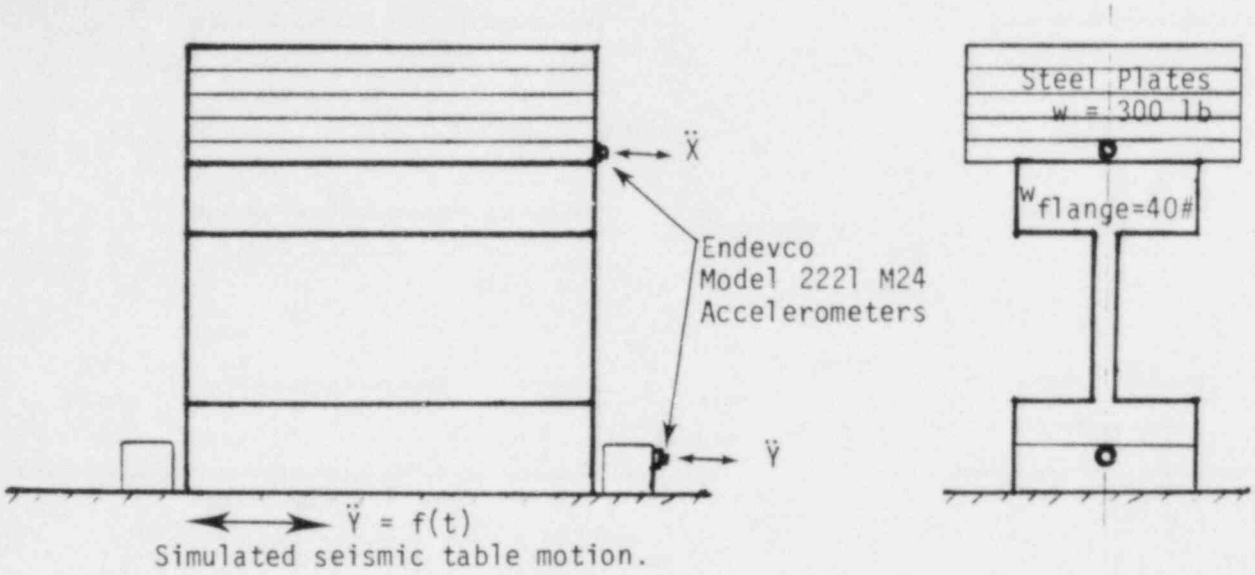

a. One-story structure

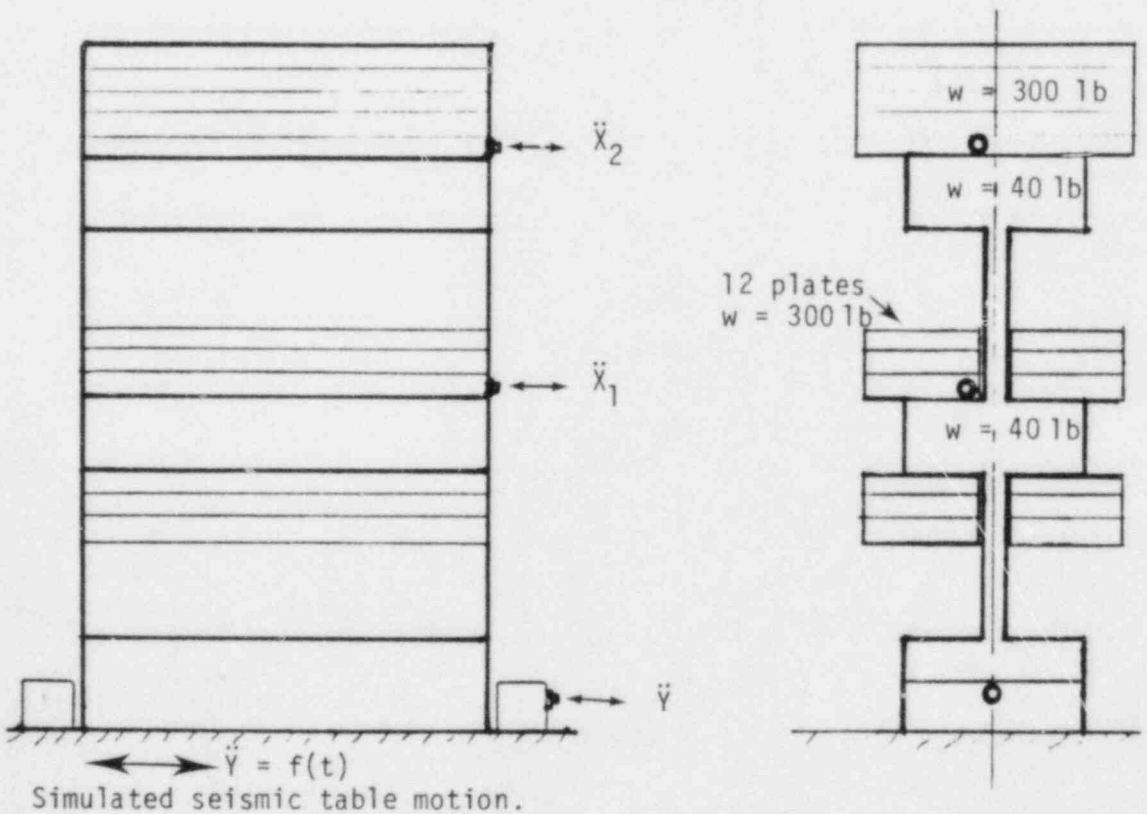

b. Two-story structure

Fig. 24. Load distribution and location of principal accelerometers.

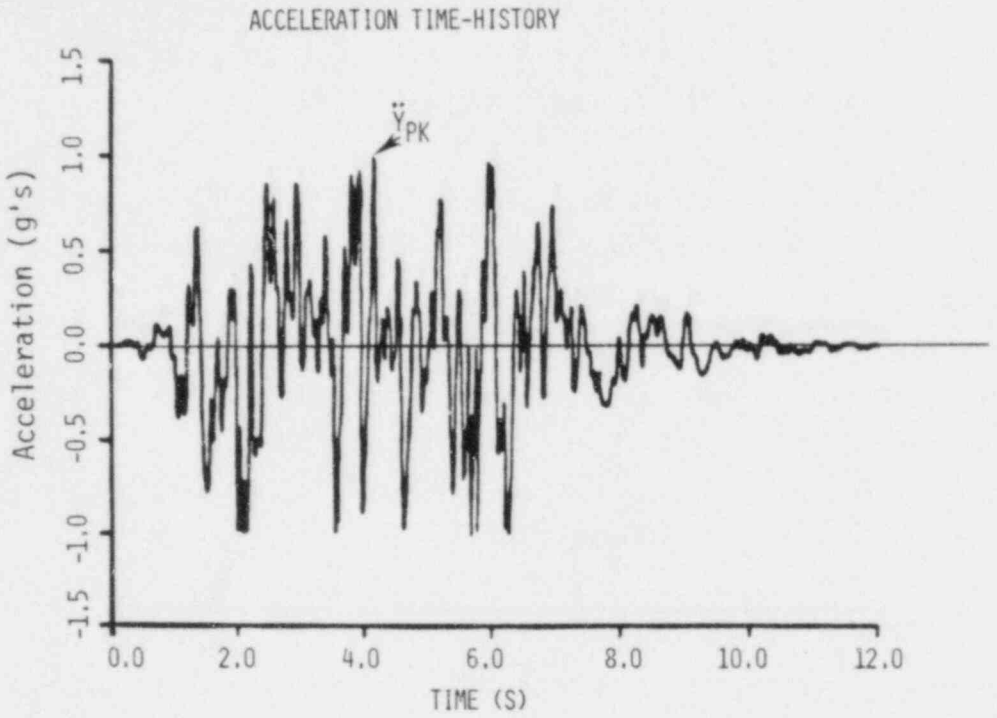

Fig. 25a. EE1 accelerogram.

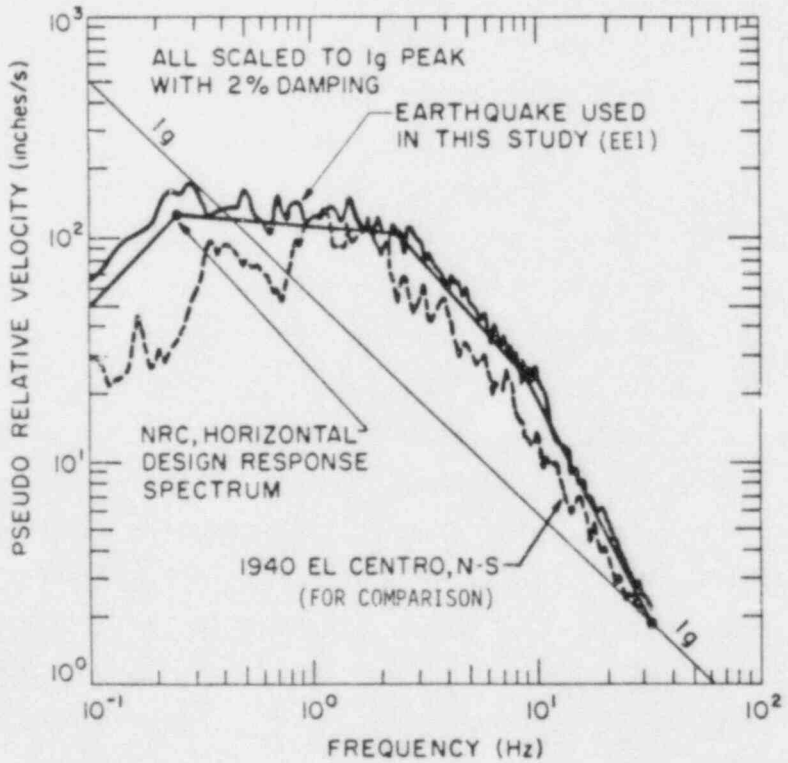

Fig. 25b. Linear response spectrum for EE1 accelerogram.

3. N_t = 19.85; this is designated as EE1 x 20 with a duration of 0.61 s. and having a frequency content up shifted by a factor of 19.85.
4. N_t = 53.0 this is designated as EE1 x 50 with a duration of 0.23 s, and having a frequency content up shifted by a factor of 53.

A typical test sequence is outlined below.

1. A structure is mounted on the shaker. Accelerometers and displacement gauges are mounted and calibrated. All calibration data is recorded on tape.
2. The desired test signal (EE1 x 5, EE1 x 10, EE1 x 20, or EE1 x 50) and the peak input acceleration ($\ddot{Y}_{pk}$, Fig. 25a) are selected.
3. The shaker is driven with a wide-band, low-amplitude signal selected to excite all major resonances in the test structure and the shaker system. This test is referred to as the system self test and is necessary because the shaker control system must compute an appropriate transfer function before it can successfully execute the desired command signal (EE1 x 5, etc.). Data are tape recorded from all transducers (accelerometers and displacement gauges) during this system self test.
4. The shaker is driven to produce the desired accelerogram (EE1 x 5, etc.). Data are tape recorded.
5. After visual inspection of the structure and preliminary analysis of the data, the structure may be removed, or if there is no apparent damage, the structure may be retested using any of the four accelerograms at any desired amplitude level. A damaged structure may also be retested after damage is noted in order to investigate the effect of a seismic event on a previously damaged structure.

All simulated seismic tests were performed on the ± 20,000-pound-force electrodynamic shaker located at K-site at Los Alamos National Laboratory.

Data reduction consisted of a number of steps outlined below. Immediately following each test, the accelerometer data [response acceleration ($\ddot{X}_1$ and $\ddot{X}_2$), and input acceleration ($\ddot{Y}$)] were analyzed using a Gen Rad Model 2507, Structural Analysis System. Transfer functions were used to determine resonant frequencies. Figure 26 is a reproduction of the transfer-function plots from the first system self test conducted on the two-story structure (No. 2-2).

From these data we conclude that the first and second modal frequencies for this specimen in the "new" condition are approximately 55 and 200 Hz. Figure 27 is a reproduction of the transfer-function plots from a test in which this same two-story structure (No. 2-2) was subjected to the simulated earthquake EE1 x 50 with a peak acceleration level ($\ddot{Y}_{pk}$) of 0.46 g's. Note that when subjected to this particular earthquake, the first mode frequency is slightly lower than was indicated from the lower-level broad-band test in the new condition; however, the second mode frequency is essentially unchanged.

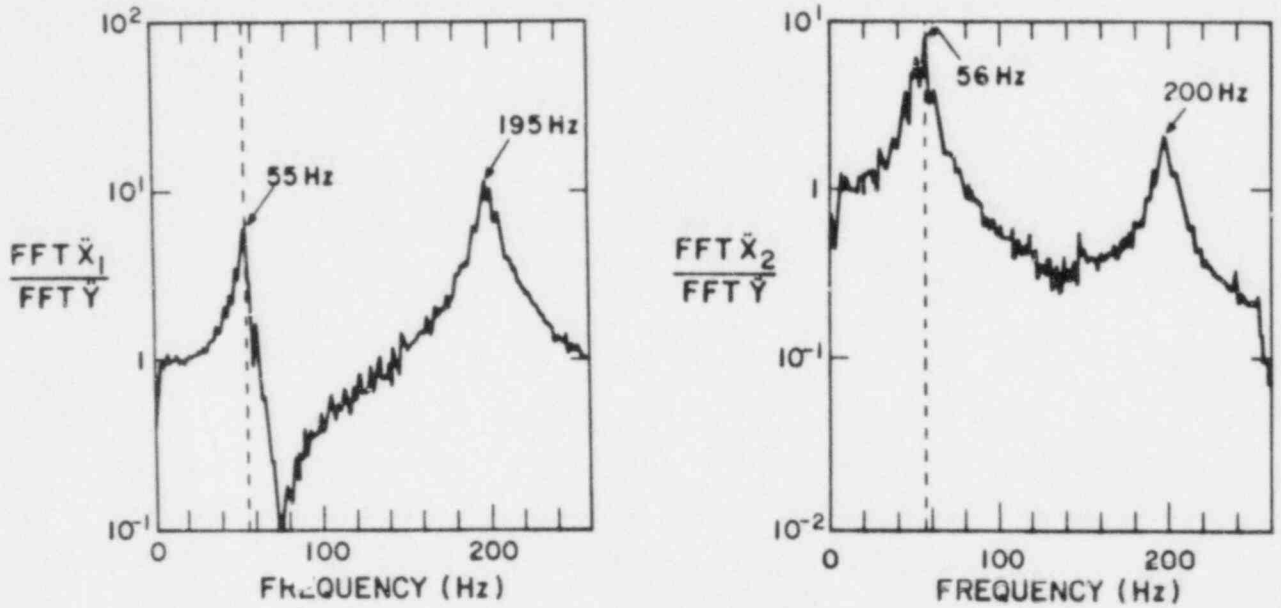

Fig. 26. Transfer function, first system self test, Model No. 2-2.

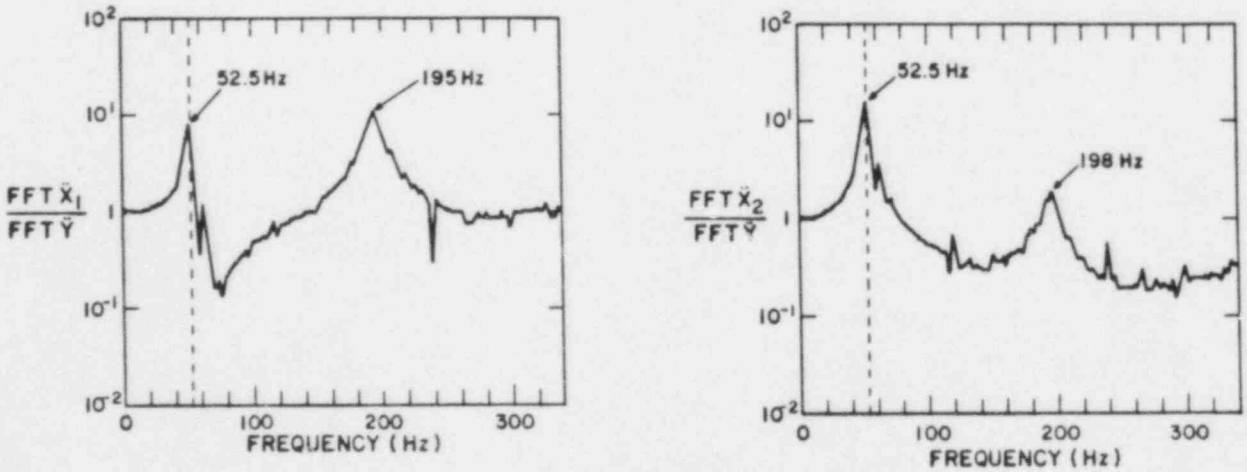

Fig. 27. Transfer function, EE1 x 50, $\ddot{Y}_{PK}$ = 0.46 g's, Model No. 2-2.

Inspection of this model following the test described above failed to reveal any visible cracks. By repeating the system self test, it was determined that the first mode frequency, as determined by a low-level, broad-band test, had been slightly reduced from 55 to 52 Hz; however, the second mode frequency remained unchanged.

This model was retested several times by subjecting it to simulated earthquake signals having progressively higher peak-acceleration levels. Figure 28 shows the transfer-function plots from a test in which this model was subjected to the EE1 x 50 earthquake with a peak acceleration level of 1.97 g's. At this input acceleration level, the apparent first mode frequency is reduced to 32.5 Hz, and there is no predominent second mode frequency. Following this test, inspection failed to reveal any visible cracks. However, when the low level, broad-band system self test was repeated, the modal frequencies were found to be significantly reduced; the first mode frequency from an original value of 55 Hz to a value of 32.5 Hz, and the second mode frequency from an original value of 200 Hz to a value of 140 Hz. Clearly, this structure has undergone a decrease in equivalent stiffness and the change is permanent. Figure 29 shows the transfer-function plots from the final test on this structure in which the peak-acceleration level was raised to 16.9 g's. Note that the structure responds with a large number of modes; it is indeed a many degree-of-freedom system. Figure 30 is a photograph of this model following this test; the cracks shown pass through the wall.

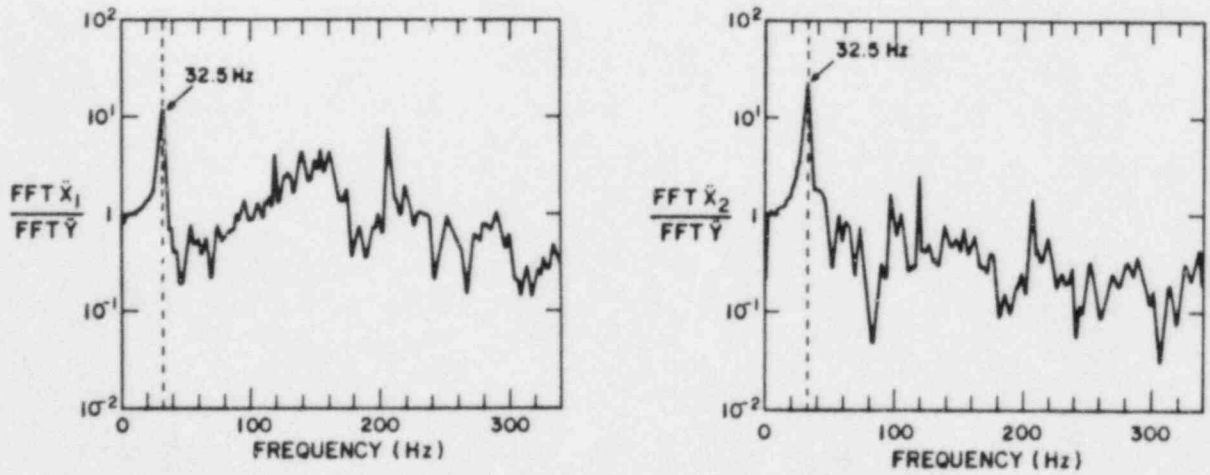

Fig. 28. Transfer function, EE1 x 50, $\ddot{Y}_{PK}$ = 1.97 g's, Model No. 2-2.

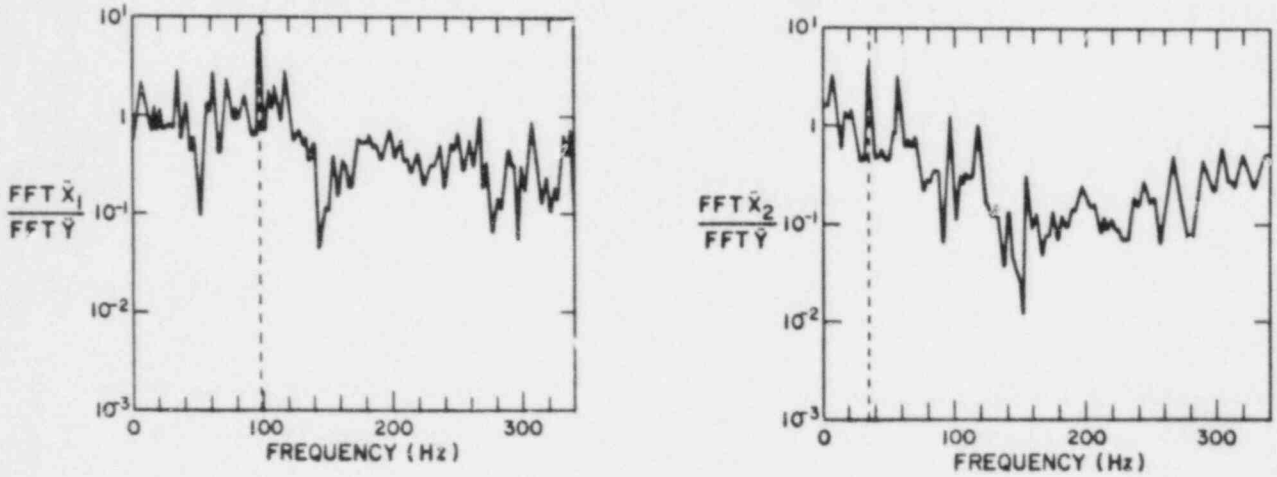

Fig. 29. Transfer function, EE1 x 50, $\ddot{Y}_{PK}$ = 16.9 g's, Model No. 2-2.

The data analysis, which was discussed above, and which used model No. 2-2 as an example, was performed immediately after each test on a given model. Additional data analysis was accomplished "off line" by playing all recorded data from the tape into a Norland 3001 analysis system. This made available the displacement and acceleration time records at each measurement point and, from these, peak displacements and accelerations were measured, and displacement and acceleration amplification factors computed. Figures 31-33 are examples of time plots from the data taken during a single test on model No. 23, a single-story structure. Values of response displacement and acceleration can be compared with values predicted by the usual linear response spectrum and appropriate nonlinear method.

The data taken from the tests of model Nos. 21 and 23 are listed in Tables VI and VII. These data indicate that, with sufficiently low input acceleration levels, the walls behave as linear, elastic structures over a wide range of frequency ratios. For example, consider model No. 23 subjected to the simulated earthquakes EE1 x 5 with $\ddot{Y}_{pk}$ = 0.34 g's, EE1 x 10 with $\ddot{Y}_{pk}$ = 0.69 g's, and EE1 x 50 with $\ddot{Y}_{pk}$ = 0.46 g's. Inspecting these data points in Table VII, we find that the effective resonance (f_e) during these tests was essentially the same as the value measured in a low-level test (f_1). This indicates that the system did not soften (hence, a linear system) and that the resonant frequency measured after the test (f_p) was essentially

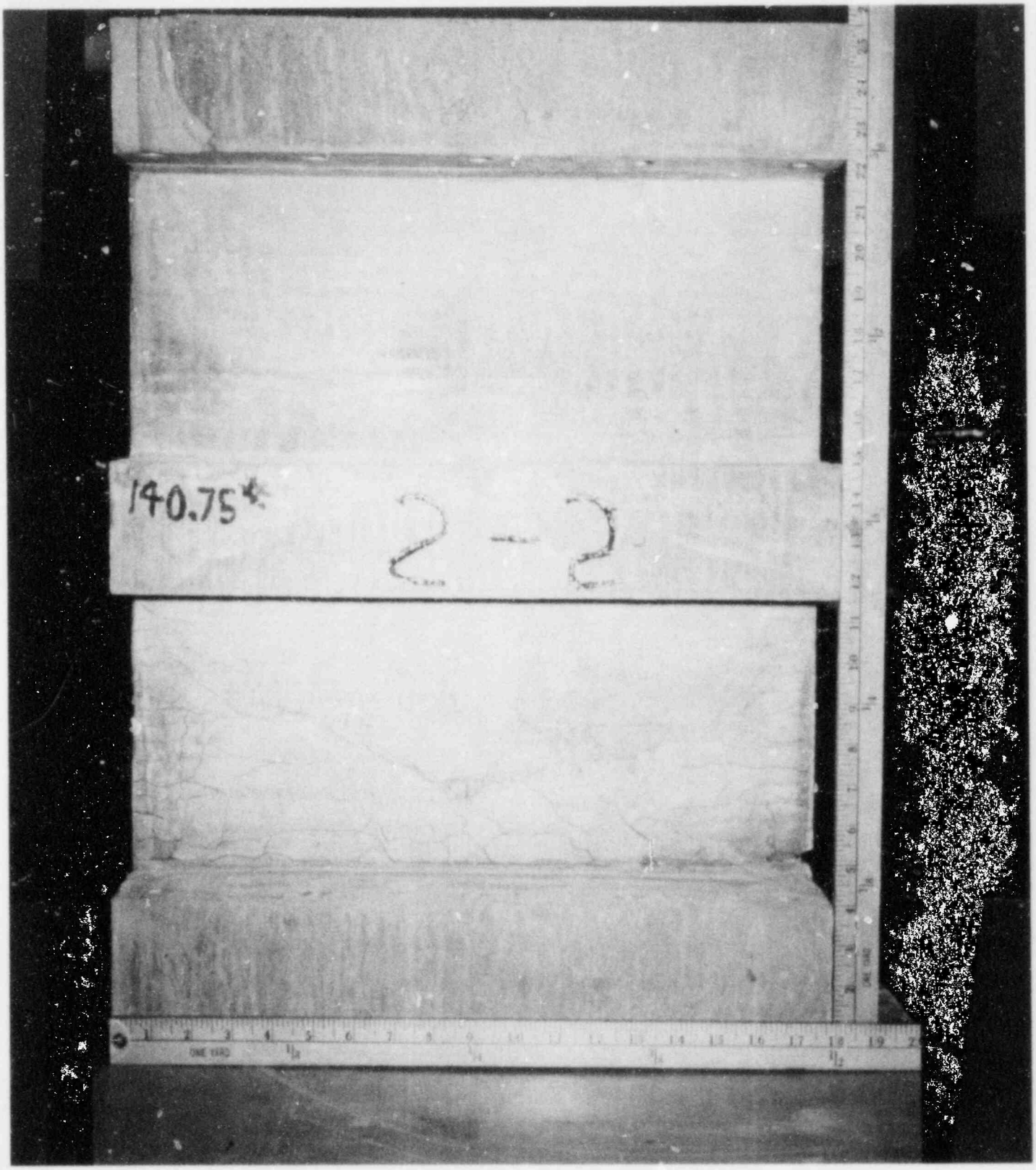

Fig. 30. Two-story shear wall structure after testing.

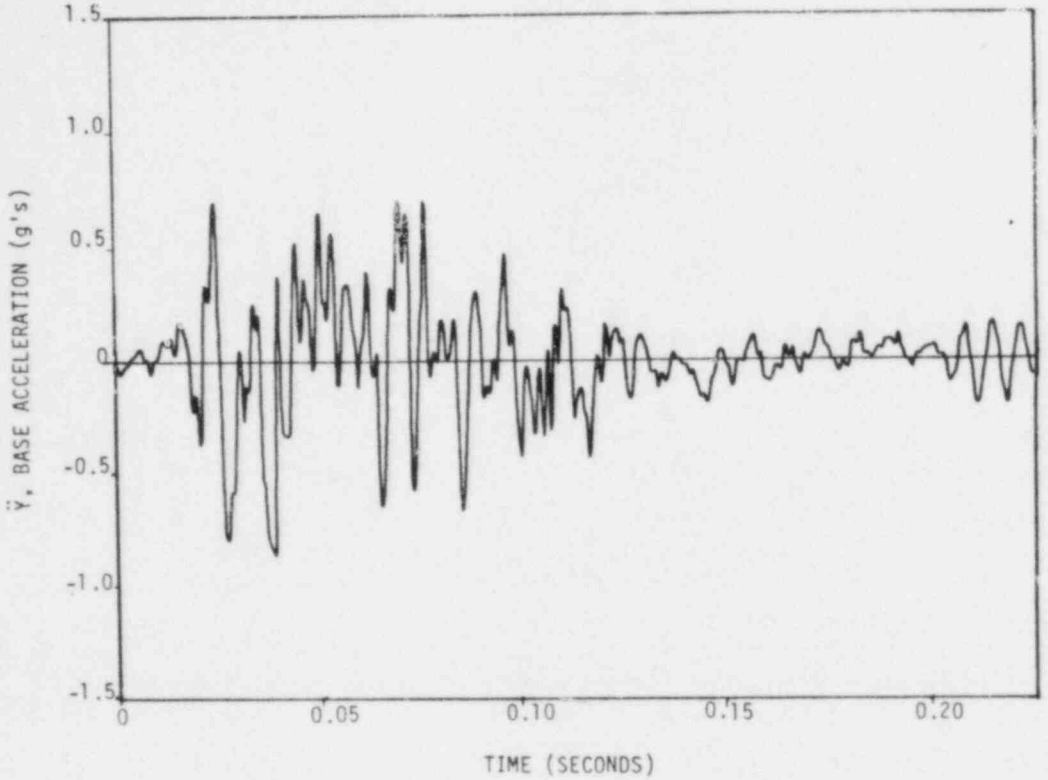

Fig. 31. $\ddot{Y}$ vs time, EE1 x 50, $\ddot{Y}_{PK}$ = -0.94 g's, Model No. 23.

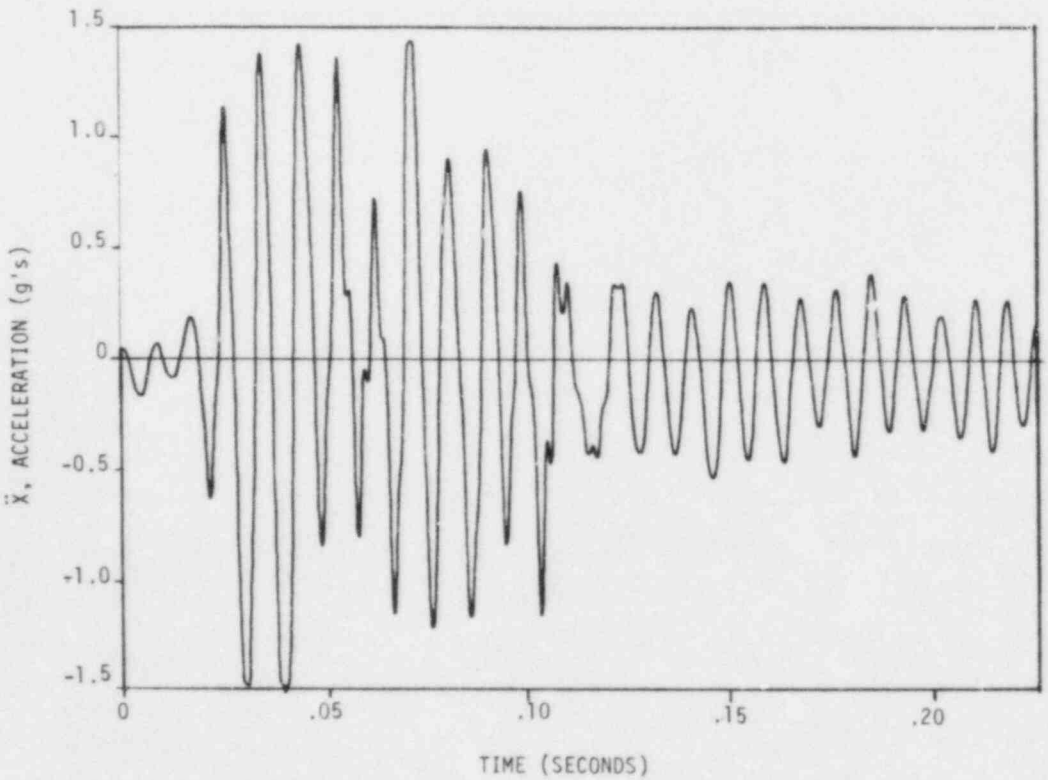

Fig. 32. $\ddot{X}$ vs time, EE1 x 50, $\ddot{X}_{PK}$ = -1.54 g's, Model No. 23.

unchanged (hence, an elastic system). However, with higher input accelerations, the system becomes nonlinear and inelastic. For example, in Table VII for test EE1 x 20 with $\ddot{Y}_{pk}$ = 2.7 g's, we see that $f_1 > f_e$ and $f_p < f_1$. Data from tests on model No. 21 lead to these same observations.

We also note that when the structure responds in a linear manner (as indicated by the fact that $f_e \approx f_1$), the measured value of peak relative displacement (u) is less than the linear displacement limit (Δ) determined by the quasistatic tests (Table IV). When the response is nonlinear (as indicated by the fact that $f_e < f_1$), the measured value of peak relative displacement (u) is greater than the linear displacement limit (Δ). As an example, consider model No. 21 subjected to EE1 x 50 with $\ddot{Y}_{PK}$ = 6.02 g's (last entry in Table VI). In this case u = 15.1 x 10^{-3} inches, which is approximately four times the quasistatically determined linear limit (Δ) of 3 to 4 x 10^{-3} in.

In the elastic response region, the effective stiffnesses computed from the measured apparent resonant frequencies ($K_{e,\ eff}$ in Tables VI and VII) for tests in which $f_e \approx f_1$, are less than the values of stiffness modulus determined from the quasistatic test data (K_1 in Table IV). However, the values of $K_{e,\ eff}$ in the linear region are larger than the values of equivalent stiffness (K_e) determined from the low-load-level, sine-sweep tests (Table V).*

The standard linear response spectrum diagram for any given earthquake can be nondimensionalized by plotting the appropriate response ratio, for example, $\ddot{X}_{PK}/\ddot{Y}_{PK}$ vs the ratio of the structure's natural frequency (ω_1) to the characteristic earthquake frequency (θ). Figure 34 is the nondimensionalized linear response spectrum, for the earthquake signal used in this study. In constructing this spectrum, θ, the earthquake characteristic frequency, was taken as 2π x 1.9 = 11.94 rad/s. This is the peaking frequency for the power spectral density plot of this earthquake signal. However, the choice of θ is arbitrary, provided that the value selected is used only for the construction of nondimensionalized response spectrum of that particular accelerogram or frequency-scaled versions thereof. The measured response ratios

*Specimen 10 is an exception; see the discussion in Sec. IV of this report for an explanation.

TABLE VI

MODEL 21 - SIMULATED SEISMIC TEST RESULTS

Test Designation	Peak Input Acceleration	Specimen Resonant Frequency[a]			Acceleration Response Ratio	Relative Displacement Maximum	ω_1/θ[b]	K eff ($lb/in. \times 10^6$)[c]	
		Pretest	During Test	Post Test					
	$\ddot{Y}_{PK}$ (g's)	f_1 (Hz)	f_e (Hz)	f_p (Hz)	$\ddot{X}_{PK}/\ddot{Y}_{PK}$	u (in. x 10^{-3})	$2\pi f_1/v$	$K_{1,eff}$	$K_{e,eff}$
EE1 x 5	0.35	111	111	105	1.7	1.2	11.8	0.43	0.43
EE1 x 10	0.55	105	106	104	1.7	1.3	5.53	0.38	0.39
EE1 x 10	1.19	103	105	104	1.5	2.1	5.42	0.37	0.38
EE1 x 10	2.48	105	99	104	1.6	5.4	5.52	0.38	0.34
EE1 x 20	0.53	107	106	105	1.7	2.0	2.83	0.40	0.39
EE1 x 20	0.88	104	104	105	1.9	2.0	2.75	0.38	0.38
EE1 x 20	2.16	104	93	105	2.0	8.0	2.75	0.38	0.30
EE1 x 50	0.63	105	105	103	1.8	2.1	1.04	0.38	0.38
EE1 x 50	1.28	105	99	105	2.0	3.2	1.04	0.38	0.34
EE1 x 50	3.42	105	88	105	1.7	9.6	1.04	0.38	0.27
EE1 x 50	3.83	105	88	105	1.6	10.2	1.04	0.38	0.27
EE1 x 50	6.02	105	85	100	1.4	15.1	1.04	0.38	0.25

[a] f_1 is determined by the low-level, broad-band system self test that precedes each simulated seismic test; f_e is the effective resonant frequency during the test taken as the frequency at which the transfer function (FFT $\ddot{X}$/FFT $\ddot{Y}$) is maximum. f_p is determined from the system self test following each simulated seismic test.

[b] For a given test signal, θ is the value of the arbitrarily selected characteristic frequency of the original earthquake ($2\pi \times 1.9 = 11.94$ radians/s) times the factor by which the original signal has been frequency scaled, N_θ. Hence, for the EE1 x 5 test, $\theta = 11.94 \times 4.96 = 59.2$ rad/s as the EE1 x 5 test signal has been frequency scaled by a factor of 4.96.

[c] The effective stiffness (Keff) is computed as $K_{1,eff} = (2\pi f_1)^2 M = (2\pi f_1)^2 \times (300+40)/386$ and $K_{e,eff} = (2\pi f_e)^2 \times (300 + 40)/386$.

TABLE VII

MODEL 23 - SIMULATED SEISMIC TEST RESULTS

Test Designation	Peak Input Acceleration	Specimen Resonant Frequency[a]			Acceleration Response Ratio	Relative Displacement Maximum	ω_1/θ[b]	K eff (lb/in.x10^6)[c]	
		Pretest	During Test	Post Test				$K_{1,eff}$	$K_{e,eff}$
	$\ddot{Y}_{PK}$ (g's)	f_1 (Hz)	f_e (Hz)	f_p (Hz)	$\ddot{X}_{PK}/\ddot{Y}_{PK}$	u (in.x10^{-3})	$2\pi f_1/\theta$		
EE1 x 5	0.34	115	115	115	1.51	1.2	12.2	0.46	0.46
EE1 x 10	0.69	115	115	115	1.37	1.4	6.05	0.46	0.46
EE1 x 10	1.21	108	112	112	1.27	1.5	5.68	0.41	0.44
EE1 x 10	3.46	108	110	112	1.26	3.9	5.68	0.41	0.42
EE1 x 20	0.95	112	108	112	1.62	2.6	2.97	0.44	0.41
EE1 x 20	1.88	112	106	108	1.84	5.3	2.97	0.44	0.39
EE1 x 20	2.70	115	99	112	1.85	6.5	3.05	0.46	0.34
EE1 x 20	4.10	112	93	102	1.60	6.7	2.97	0.44	0.30
EE1 x 50	0.46	115	115	115	2.26	1.7	1.14	0.46	0.46
EE1 x 50	0.54	115	115	108	1.92	1.7	1.14	0.46	0.46
EE1 x 50	0.94	112	108	108	1.64	2.6	1.11	0.44	0.41
EE1 x 50	2.34	108	107	115	1.89	4.9	1.07	0.41	0.40
EE1 x 50	4.77	102	96	110	1.46	8.1	1.10	0.36	0.32
EE1 x 50	10.70	110	73	105	1.17	3.4	1.09	0.42	0.19
EE1 x 50	13.80	105	58	100	0.86	4.7	1.04	0.38	0.12
EE1 x 50	20.80	100	58	90	0.64	6.2	0.99	0.35	0.12

[a] f_1 is determined by the low-level, broad-band system self test that precedes each simulated seismic test; f_e is the effective resonant frequency during the test taken as the frequency at which the transfer function (FFT $\ddot{X}$/FFT $\ddot{Y}$) is maximum. f_p is determined from the system self test following each simulated seismic test.

[b] For a given test signal, θ is the value of the arbitrarily selected characteristic frequency of the original earthquake (2π x 1.9 = 11.94 radians/s) times the factor by which the original signal has been frequency scaled, N_θ. Hence, for the EE1 x 5 test, θ = 11.94 x 4.96 = 59.2 rad/s as the EEL x 5 test signal has been frequency scaled by a factor of 4.96.

[c] The effective stiffness (Keff) is computed as $K_{1,eff} = (2\pi f_1)^2 M = (2\pi f_1)^2$ x (300+40)/386 and $K_{e,eff} = (2\pi f_e)^2$ x (300 + 40)/386.

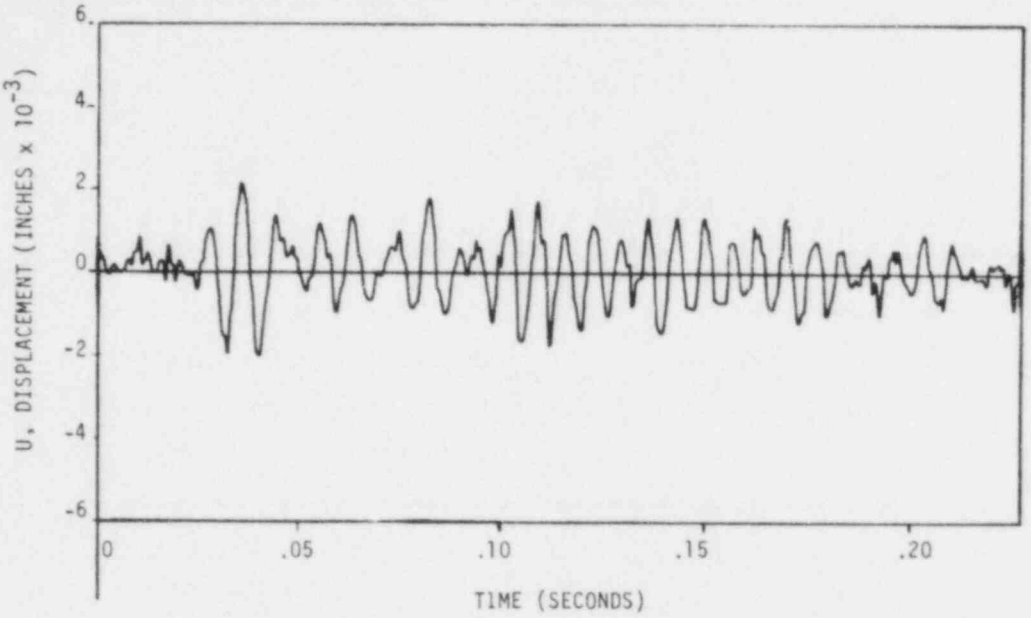

Fig. 33. Displacement (u) vs time, EE1 x 50, Model No. 23, U_{max} = 0.0026 in.

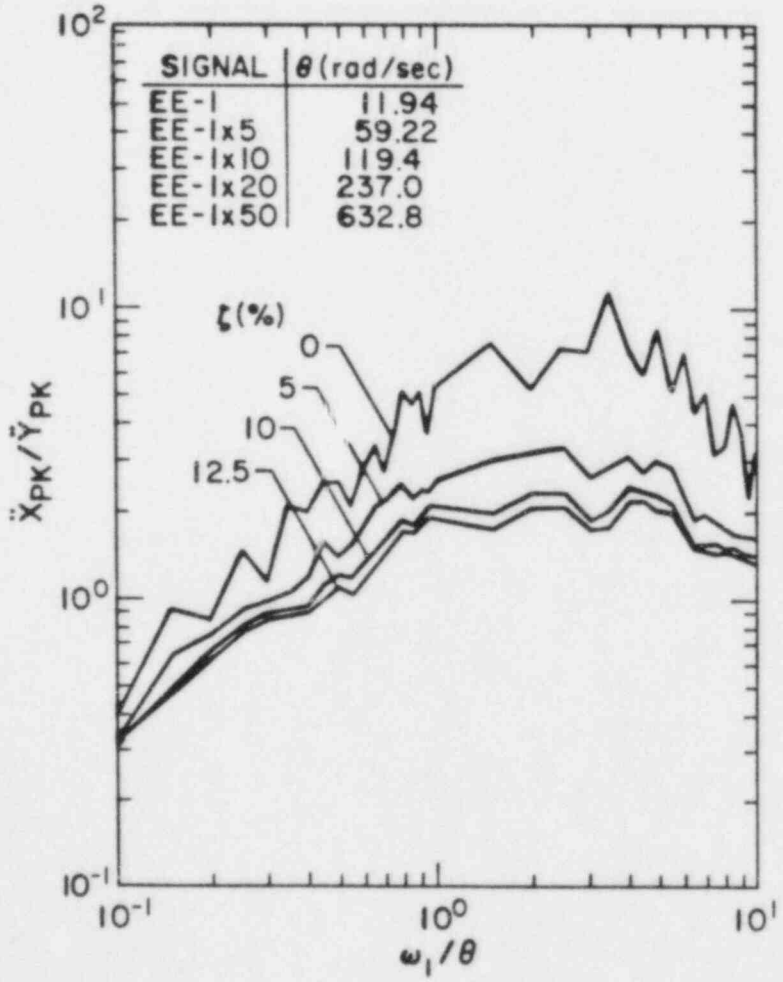

Fig. 34. Nondimensionalized, linear, acceleration response spectrum.

obtained from the tests on model Nos. 21 and 23 are plotted on Figs. 35 and 36. From these plots we observe that if a linear response spectrum were used to predict the response of these structures, an equivalent viscous damping ratio (ζ) of at least 12.5% would be appropriate. In addition, we observe that when these structures have been loaded well into the nonlinear, inelastic region, the response is reduced to values even lower than predicted using this relatively large amount of damping. Consider the following examples: for model No. 21, tests EE1 x 50 with $0.63 \leq \ddot{Y}_{PK} \leq 6.02$ g's plotted at $\omega_1/\theta \approx 1$ on Fig. 35, and for model No. 23, tests EE1 x 50 with $0.46 \leq \ddot{Y}_{PK} \leq 20.8$ g's plotted at $\omega_1/\theta \approx 1$ on Fig. 36. Nonlinear response theory predicts this result. Figure 37 depicts the expected trend. Note that for a given structure with an initial resonant frequency (ω_1) and subjected to a given earthquake (characterized by θ), the value of ω_1/θ is fixed. In this case there is a certain threshold for input amplitude ($\ddot{Y}_{PK}$) below which response is linear. Beyond this threshold, as $\ddot{Y}_{PK}$ is increased, the response ratio ($\ddot{X}_{PK}/\ddot{Y}_{PK}$) decreases. The exact shape of the nonlinear response spectra curves depends upon several system parameters, the most obvious of which is the curvature of the structure's force vs deformation relationship.

The data from the tests conducted on the two-story structure, model No. 2-2, are tabulated and plotted in essentially the same manner as has been described in the preceding paragraphs. Table VIII gives some of the data taken during tests conducted on model No. 2-2. The data taken from tests in the structure's linear, elastic range are plotted on a linear design response spectrum with a damping ratio of 12.5% in Fig. 38. Even in the linear elastic range this two-story structure responds as if the equivalent damping is more than 12.5%. Nonlinear response further decreases the second-floor response ratio ($\ddot{X}_2/\ddot{Y}_{PK}$). See the data point marked "X_2-Final" on Fig. 38. Nonlinear analysis of the data from these tests is continuing.

VII. DISCUSSION OF RESULTS

We believe that the quasistatic tests, conducted on structures identical to the structures used in the dynamic tests, were very worthwhile. The values

TABLE VIII

MODEL 2-2 - SIMULATED SEISMIC TEST RESULTS

Test Region	Test Designation	$\ddot{Y}_{PK}$ (g's)	Structure Resonant Frequency $f_{1,L}$[2] (Hz)	$f_{1,u}$[2] (Hz)	$f_{e,L}$[2] (Hz)	$f_{e,u}$[2] (Hz)	$f_{p,L}$[2] (Hz)	$f_{p,u}$[2] (Hz)	Response Ratio $\ddot{X}_{1PK}/\ddot{Y}_{PK}$	$\ddot{X}_{2PK}/\ddot{Y}_{PK}$	ω_{1i}/θ[1]
A, Linear Elastic	EE1 x 5	0.37	55	195	55	--	55	194	1.08	1.45	12.0
	EE1 x 10	0.66	55	194	53	195	53	198	1.40	2.23	5.95
	EE1 x 20	0.55	53	198	53	195	55	198	1.19	1.71	3.00
	EE1 x 50	0.46	55	198	53	198	52	194	1.19	2.28	1.12
B, Nonlinear	EE1 x 50	1.97	35	145	32	155	35	138	1.36	1.80	1.12
	EE1 x 50	4.26	30	112	27	116	30	111	1.69	1.25	1.12
	EE1 x 50	7.62	30	111	27	119	29	99	1.31	1.18	1.12
	EE1 x 50	16.90	29	99	--	--	--	--	1.04	0.57	1.12

(1) ω_{11} is the initial resonant frequency for the first-story wall and attached mass. It is taken as 2π x 113 = 710 radians/s which is the average value measured for the two single-story models, that is, ω_1 of model 21 was (2π x 115) rad/s and ω_1 of model 23 was (2π x 111) rad/s.

(2) f_1, f_e, and f_p have same meaning as given to Tables VI and VII. The second subscripts, L and u ($f_{1,L}$ and $f_{1,u}$ for example) designate the first (or lower) and second (or upper) modal frequencies respectively.

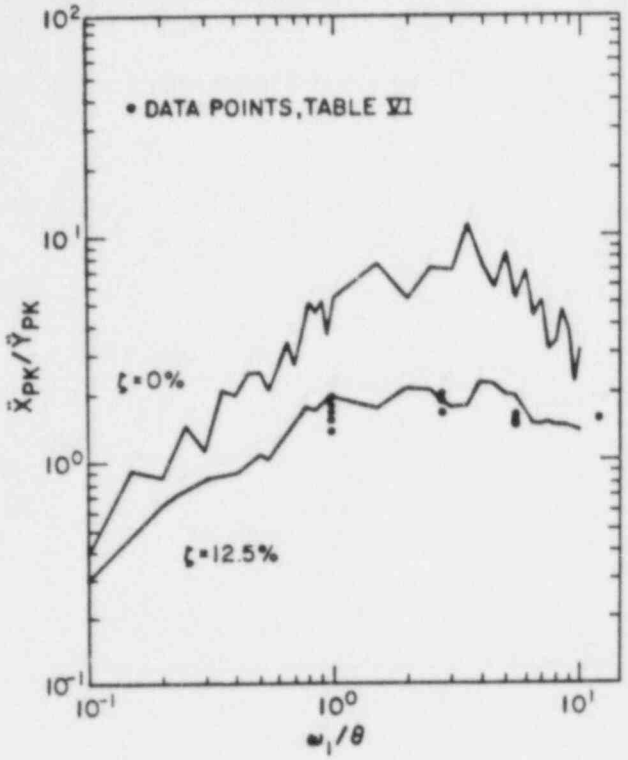

Fig. 35. Experimentally determined response spectrum, Model 21.

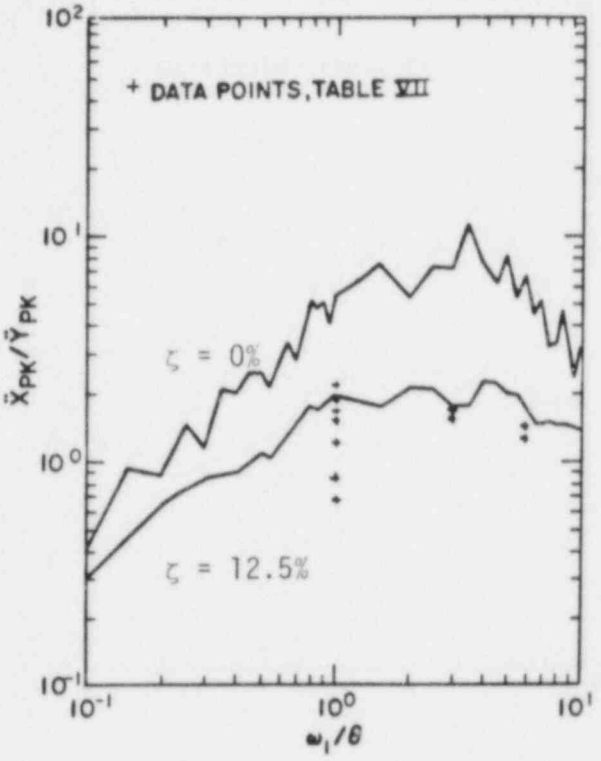

Fig. 36. Experimentally determined response spectrum, Model 23.

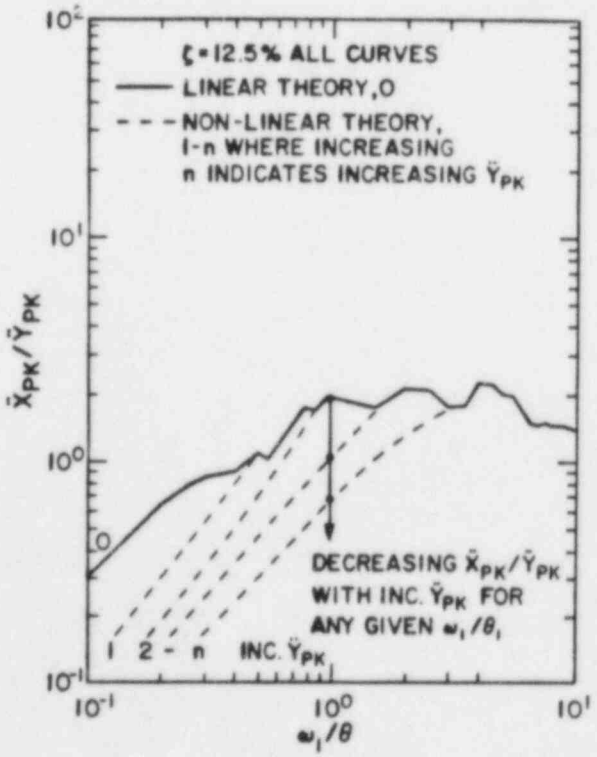

Fig. 37. Nonlinear effects.

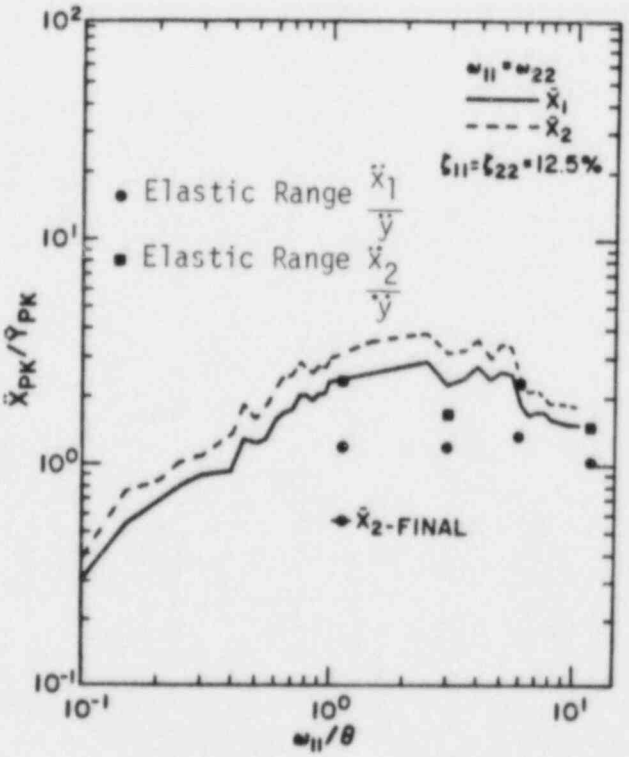

Fig. 38. Experimental data (Model 2-2) on a linear design response spectrum.

of stiffness, apparent linear limit, and ultimate strength for this particular structure that were obtained from these quasistatic tests, appear to be essential base line data points. Although the quasistatic load-cycling tests did not duplicate the actual load-cycling history that results from seismic response, the tests gave valuable information about the hysteretic energy loss and how the amount of that loss is affected by load level (Table III). This appears to be essential information for the construction of a good theoretical model of this structure. For these reasons, we plan to conduct quasistatic load (monotonic and cyclic) tests on the box-shaped structures that will be tested in the second phase of this program.

Classical methods of harmonic vibration testing (sine sweep and resonance search) are not recommended for evaluation of reinforced-concrete structures if the results are to be used in predicting the structure's response to seismic excitation. That is because even at low load levels, tests that subject the structure to many more cycles than it will experience in seismic response yield results that may be predominately dependent upon the stiffness degradation caused by load cycling. As the load level in such tests increases, the value of experimental results is even more questionable since most of the theories used to interpret the results are based on the assumption that the response is steady state; with a nonlinear, hysteretic structure, there is no steady-state response.

For these reasons, no further harmonic motion tests will be conducted as part of this project; however, as a separate research effort it might be worthwhile to investigate the effect of long-term, low-level vibration (such as might be produced by operating equipment) on the stiffness degradation of reinforced-concrete structures.

Unlike the harmonic motion tests, the simulated seismic tests were found to be very informative. These tests subject the structure to a load history involving a limited number of nonsymmetrical load cycles. Results of the tests can best be understood and utilized in a seismic design by measuring, as directly as possible, input and response parameters that can be plotted on appropriate response spectra. With low loads, where the structure response is essentially linear, the measured response parameter can be plotted on the usual linear response spectrum. Response spectra can be computed for various amounts and types of assumed damping, and the actual effective damping can be established by comparing the plotted, measured response with these curves.

During a series of simulated seismic tests, it is possible to determine, with considerable resolution, the level of input acceleration required to produce nonlinear response and the relative degree of nonlinearity associated with a given input acceleration level. This appears to be most readily accomplished by monitoring shifts in the effective resonant frequency that occur when the input acceleration is increased. Effective resonant frequency appears to be most readily measured by analysis of the data in the frequency domain, and this analysis is readily accomplished using modern analysis equipment.

When nonlinear response is indicated, the experimental data can probably be best understood and utilized for a seismic design by plotting it on an appropriate nonlinear response spectrum. How to construct the best nonlinear response spectrum for reinforced-concrete structures using fundamental and readily measured properties has not been settled. As part of this research, we have proposed a nonlinear response spectrum constructed on the assumption that reinforced-concrete structures behave as softening, hysteretic systems. This assumption is supported by quasistatic load tests carried out as a part of this research (Fig. 12, for example) and by tests conducted by others.[2,3] The results of the simulated seismic tests that were carried into the nonlinear region support the results predicted by the proposed nonlinear spectrum. Specifically, beyond the linear response limit the acceleration response ratio ($\ddot{X}_{PK}/\ddot{Y}_{PK}$) decreases with increasing input acceleration level at a rate that cannot be adequately explained by increasing equivalent damping. Consequently, more analysis and many more tests should be performed to determine how best to construct a nonlinear response spectrum for reinforced-concrete structures. Questions that should be answered include the following:

1. What is the simplest method that might be used to adequately characterize a structure's nonlinear, softening, hysteretic load-deflection diagram? Computation from basic properties of materials (concrete and reinforcement) and geometry would be ideal, and simple (perhaps quasistatic) tests on scale models would be suitable; however, any method will have to be verified.
2. Once a structure's load-deflection diagram is established, how should it be mathematically modeled for the construction of the nonlinear response spectrum? The authors have used a simple bilinear, hysteretic model. Modifications or improvements might include better (than bilinear) nonlinear representation, more realistically shaped

hysteretic loops, stiffness degradation with load cycling at a fixed load level, inelastic action (that is, increasing permanent deformation at zero load after each load cycle). However, the results of some analyses indicate that complicated modeling may not be required provided the energy loss per cycle is adequately represented.

3. Can the characteristic frequency of an earthquake (referred to as θ in this report) be defined so that a single nondimensionalized response spectrum, which applies to several earthquakes, can be constructed? The use of the response spectrum method does not depend upon an affirmative answer to this question as a nonlinear response spectrum can be constructed for each earthquake record of interest (as is the current practice in the use of linear spectra.

Although the matter of the transition from linear to nonlinear response has been mentioned in the preceding paragraphs, this subject may warrant additional comment. All of the structures subjected to simulated seismic tests were subjected to a series of accelerograms of increasing peak acceleration, after each of which the structure was visually inspected for signs of damage. With all three structures, it was determined that a noticeable change in effective stiffness ($K_{e,\ eff}$, Tables VI and VIII) had occurred before any visible cracking occurred. For example, the effective stiffness ($K_{e,\ eff}$) of model No. 21 had been reduced from 0.43×10^6 to 0.30×10^6 lbs/in., a reduction in stiffness of 30%, without any visible cracking. With model No. 23, the effective stiffness had been reduced by 34% (from 0.46×10^6 to 0.30×10^6 lbs/in.) before cracking was visible. These results indicate that visual inspection of reinforced-concrete structures may not be adequate to determine whether or not a structure has been loaded into its nonlinear response region by a past earthquake.

VII. CONCLUSIONS

Although the primary purpose of the Phase-I tests discussed in this report was the preparation for tests on more complicated structures, the results lead to several conclusions that are of immediate interest.

1. The linear region lateral stiffness of these shear walls, as determined by quasistatic tests, was significantly smaller than the value computed using elementary mechanics principles. Computed values of

stiffness ranged from 2.33 x 10^6 to 3.03 x 10^6 lbs/in. (Table IV). It is certainly true that, because there is no truly linear region in the load-deformation diagram, the measured value of stiffness is dependent upon what value of load (or deformation) is selected as the linear limit and how the slope of that region is determined. However, the only possible way to increase these measured values of stiffness by a factor of almost 3, which would be necessary to coincide with the calculated values, would be to define the stiffness as the near zero load slope. This certainly is not desirable as the computed stiffness is used to predict response over a reasonably large linear loading range. The effective linear range stiffness values determined by simulated seismic tests were even smaller than those determined by the quasistatic tests (0.43 x 10^6 lbs/in. for specimen No. 21 and 0.46 x 10^6 lbs/in. for specimen No. 23, Tables VI and VII). The discrepancy between computed and measured stiffness has also been noted by Japanese and French investigators.[6,7] The Japanese, who used square box-shaped test structures in their testing program, attributed the lower observed stiffnesses to shear lag in the compression and tension walls and/or to effects of microcracking in the concrete shear walls. Because shear lag is not a consideration in single shear walls, we conclude that nonvisible microcracks in the virgin specimens may have significant effects upon the stiffness. Further, it is possible that these cracks grow and render the stiffness further reduced even when only a few low-level load cycles are applied. These findings certainly cause considerable concern about our ability to predict a reinforced-concrete structure's modal frequencies using either computed or measured (from static tests) values of stiffness.

2. The cracking strengths (V_{CR}) of these shear walls computed using the methods given in The American Concrete Institute (ACI)-349 ranged between 3650 and 3770 lbs (Table IV). These values are in reasonable agreement with the observation that, in the quasistatic tests, appreciable nonlinear behavior began at about 3500 lbs.
3. The ultimate strengths (Vu) of these shear walls computed using the methods specified in ACI-349 ranged between 4870 and 5630 lbs. These values proved to be somewhat conservative as compared with the values of maximum load (F_{ULT}) measured during the quasistic tests (Table IV).

4. The quasistatic cyclic-load tests clearly indicated the significant increase in hysteretic energy loss with increasing load level. Converting these measured values of energy loss into values for equivalent viscous damping coefficients (ζ) demonstrates that then these specimens are cycled at high load loads we can expect very large equivalent damping (up to 20%) from this hysteretic effect (Table III). This finding was confirmed by the simulated seismic tests, in which the linear region response was identified and predicted by assigning the equivalent damping ratio of 12.5%, and the nonlinear region response was characterized by even larger equivalent damping (Figs. 35, 36, and 38).

ACKNOWLEDGEMENTS

The authors wish to thank the Los Alamos Analysis and Test Group, WX-11, for the use of their facilities and staff and, in particular, for the assistance of Norman Hunter, Ted Crawford, Rick DeWitt, and John Greeman.

REFERENCES

1. E. Endebrock, R. Dove, and C. A. Anderson, "Margins to Failure - Category I Structures Program: Background and Experimental Program Plan," Los Alamos National Laboratory report LA-9030-MS, NUREG/CR-2347 (September 1981).

2. R. G. Oesterle, A. E. Fiorato, L. S. Johal, J. E. Carpenter, H. G. Russell, and W. G. Corley, "Earthquake Resistant Structural Walls--Tests of Isolated Walls," Report to National Science Foundation by the Portland Cement Association, Skokie, Illinois, November 1976 (NTIS Accession No. PB271467/AS).

3. R. G. Oesterle, J. D. Ariztizabal-Ochoa, A. E. Fiorato, H. G. Russell, and W. G. Corley, "Earthquake Resistant Structural Walls--Tests of Isolated Walls-Phase II," Report to National Science Foundation by the Construction Technology Laboratories, a Division of the Portland Cement Association, Skokie, Illinois, October 1979 (NTIS Accession No. PB80-132418).

4. H. G. Harris, G. M. Sabnis, and R. N. White, "Reinforcement for Small Scale Direct Models of Concrete Structures," paper SP 24-6 in Models for Concrete Structures, (American Concrete Institute, Detroit, Michigan, 1970), ACI Publication No. 24. pp. 141-158.

5. J. E. Ruzicka and T. F. Derby, Influence of Damping in Vibration Isolation, (Shock and Vibration Information Center, US Department of Defense, SVM-7, Naval Research Laboratory, Washington, DC, 1971).

6. H. Umemura, H. Aoyama, M. Ito, and Y. Hasakawa, "Aseismic Characteristics of RC Box and Cylinder Walls," Sixth World Conference on Earthquake Engineering, New Delhi, India, January 1977 (Sarita Prakashar, 1977), pp. 3144-49.

7. J. Gauvain, A. Hoffmann, C. Jeandidier, and M. Linolant, "Tests and Calculations of the Seismic Behavior of Concrete Structures," Proc. Fifth International Conference on Structural Mechanics in Reactor Technology, Berlin, August 1979 (North Holland, New York, 1979).

DISTRIBUTION

	Copies
Nuclear Regulatory Commission, RD, Laurel, Maryland	273
Technical Information Center, Oak Ridge, Tennessee	2
Los Alamos National Laboratory, Los Alamos, New Mexico	50
	325

NRC FORM 335 (12 84) NRCM 1102, 3201, 3202

U.S. NUCLEAR REGULATORY COMMISSION

BIBLIOGRAPHIC DATA SHEET

SEE INSTRUCTIONS ON THE REVERSE

1 REPORT NUMBER (Assigned by TIDC and Vol. No., if any)

NUREG/CR-4274
LA-10443-MS

2 TITLE AND SUBTITLE

Analysis and Tests on Small-Scale Shear Walls
FY-82 Final Report

3 LEAVE BLANK

4 DATE REPORT COMPLETED

MONTH	YEAR
May	1985

5 AUTHOR(S)

E. G. Endebrock, R. C. Dove, W. E. Dunwoody

6 DATE REPORT ISSUED

MONTH	YEAR
September	1985

7 PERFORMING ORGANIZATION NAME AND MAILING ADDRESS (Include Zip Code)

Los Alamos National Laboratory
Los Alamos, NM 87545

8 PROJECT/TASK/WORK UNIT NUMBER

9 FIN OR GRANT NUMBER

A7221

10 SPONSORING ORGANIZATION NAME AND MAILING ADDRESS (Include Zip Code)

Mechanical/Structural Engineering Branch
Division of Engineering Technology
Office of Nuclear Regulatory Research
U.S. Nuclear Regulatory Commission
Washington, DC 20555

11a TYPE OF REPORT

Informal

b PERIOD COVERED (Inclusive dates)

12 SUPPLEMENTARY NOTES

13 ABSTRACT (200 words or less)

The Phase-I experimental program was completed during FY 1982. This report summarizes the results of (1) quasistatic (monotonic and load-cycling) tests, (2) sinusoidal vibration tests, and (3) simulated earthquake tests conducted on small-scale, reinforced-concrete shear walls. Model construction, test methods, instrumentation, and experimental results are presented in this report. Experimental results are interpreted to investigate the effects of high-load levels (which produce cracking and failure of the walls) on stiffness, damping, and on deformation and acceleration transmissibility. The nonlinear analysis method that has been developed as part of this program has been used to aid in the interpretation of these experimental results.

14 DOCUMENT ANALYSIS - a KEYWORDS/DESCRIPTORS

15 AVAILABILITY STATEMENT

Unlimited

16 SECURITY CLASSIFICATION

(This page)
Unclassified

(This report)
Unclassified

17 NUMBER OF PAGES

18 PRICE

b IDENTIFIERS/OPEN-ENDED TERMS

☆ U.S. GOVERNMENT PRINTING OFFICE 1985—576-034/20138

Available from

Superintendent of Documents
U.S. Government Printing Office
Post Office Box 37082
Washington, D. C. 20013-7982

and

National Technical Information Service
Springfield, VA 22161

Los Alamos